Agrobacterium tumefaciens divisome proteins regulate the transition from polar growth to cell division

Matthew Howell[1], Alena Aliashkevich[2], Kousik Sundararajan[3], Jeremy J. Daniel[1], Patrick J. Lariviere[3], Erin D. Goley[3], Felipe Cava[2], and Pamela J.B. Brown[1#]

[1]Division of Biological Sciences, University of Missouri, Columbia, MO, 65203

[2]Department of Molecular Biology. Laboratory for Molecular Infection Medicine Sweden (MIMS), Umeå Centre for Microbial Research, Umeå University, Umeå, Sweden

[3]Department of Biological Chemistry, Johns Hopkins University School of Medicine, Baltimore, MD 21205

[#]Address correspondence to Pamela J.B. Brown, brownpb@missouri.edu

Abstract

The mechanisms that restrict peptidoglycan biosynthesis to the pole during elongation and re-direct peptidoglycan biosynthesis to mid-cell during cell division in polar-growing Alphaproteobacteria are largely unknown. Here, we demonstrate that although two of the three FtsZ homologs localize to mid-cell, exhibit GTPase activity and form co-polymers, only one, $FtsZ_{AT}$, is required for cell division. We find that $FtsZ_{AT}$ is required not only for constriction and cell separation, but also for the termination of polar growth and regulation of peptidoglycan synthesis at mid-cell. Depletion of FtsZ in *A. tumefaciens* causes a striking phenotype: cells are extensively branched and accumulate growth active poles through tip splitting events. When cell division is blocked at a later stage, polar growth is terminated and ectopic growth poles emerge from mid-cell. Overall, this work suggests that *A. tumefaciens* FtsZ makes distinct contributions to the regulation of polar growth and cell division.

Introduction

The spatial and temporal regulation of cell division is a vital process across bacterial species with implications in the development of antimicrobial therapies [1]. The cell division process must coordinate membrane invagination(s), peptidoglycan (PG) biosynthesis and remodeling, and the physical separation of the two daughter cells, all while maintaining cellular integrity. Furthermore, cell division must be precisely regulated to be orchestrated with other key cell cycle processes including cell elongation, DNA replication, and chromosome segregation to ensure that each daughter cell is of sufficient size and contains a complete genome [2, 3].

To initiate bacterial cell division, the tubulin-like GTPase, FtsZ, polymerizes and forms a discontinuous ring-like structure at the future site of cell division [4-10]. The presence of FtsZ at mid-cell leads to the recruitment of many proteins that function in cell division, collectively called the divisome [11-14]. The divisome includes cell wall biosynthesis proteins, such as the penicillin-binding protein, PBP3, and FtsW, which contribute to PG biosynthesis and remodeling necessary to form new poles in daughter cells [11]. Once the divisome is fully assembled, FtsZ filaments treadmill along the circumference of the mid-cell, driving the Z-ring constriction [9, 10]. The movement of FtsZ filaments is correlated with the movement of enzymes that function in septal PG biogenesis. These finding are consistent with the notion that FtsZ not only recruits enzymes that function in PG biogenesis to mid-cell but also regulates their activities to promote proper cell wall biogenesis [15-17].

In most rod-shaped model organisms used to study cell division, a block in cell division leads to the production of long, smooth filamentous cells. This phenotype suggests that assembly or activation of some divisome components is necessary not only to enable the cells to divide but also to stop cellular elongation. Indeed, in *Escherichia coli*, FtsZ (along with the Z-ring stabilizing proteins FtsA, ZipA, and ZapA) has been proposed to have an early function in the switch from lateral PG biogenesis to mid-cell PG biosynthesis [18]. Following maturation of the divisome by recruitment of additional PG remodeling enzymes and cell division proteins, PG biosynthesis is coordinated with membrane invagination, enabling cells to constrict and separate [19].

Conversely to e.g. *E. coli*, polar growing rods in the alphaproteobacterial clade Rhizobiales exhibit branched morphologies when cell division is blocked [20-27]. Examination of the cell morphologies resulting from the block in cell division suggests that different types of branched morphologies arise [28]. Drug treatments that block DNA replication cause an early block in cell division, resulting in a "Y" morphology in which the branches are formed from existing growth poles [25, 26]. In contrast, antibiotics that target PBP3 cause mid-cell bulges and branches with some cells adopting a "T" or "+" morphologies [25, 27]. These observations suggest that polar-like PG synthesis is redirected to mid-cell when cell division is blocked at a later stage. The manifestation of two distinct phenotypes during early and late blocks in cell division suggests that divisome assembly and activation may contribute to termination of polar growth, onset of mid-cell PG biosynthesis, cell constriction, and ultimately cell separation.

In *Agrobacterium tumefaciens,* homologs of FtsZ and FtsA fused to fluorescent proteins localize at the growth pole during elongation and at mid-cell during division [27, 29, 30]. FtsZ was found to arrive at mid-cell considerably earlier than FtsA [30], indicating that FtsZ may be able to initiate Z-ring formation prior to FtsA recruitment to the divisome. This observation is consistent with the described order of divisome assembly in *Caulobacter crescentus* [31] and suggests that a distinctive time-dependent role of these proteins in cell division.

Here, we take advantage of the ability to deplete essential proteins in *A. tumefaciens* [32] to explore the function of cell division proteins FtsZ, FtsA, and FtsW in a polar growing alphaproteobacterium. Although the genome of *A. tumefaciens* encodes three Fts*Z* homologs, we

77 find that only one, henceforth referred to as $FtsZ_{AT,}$ is essential for cell survival. $FtsZ_{AT}$ is
78 required to recruit division proteins to mid-cell and likely regulates the activity of PG
79 biosynthesis enzymes at mid-cell. In the absence of $FtsZ_{AT}$, cells not only fail to divide but are
80 also unable to terminate polar growth. Depletion of either FtsA or FtsW also causes a block in
81 cell division, but unlike $FtsZ_{AT}$ depletion, growth at the poles is halted and instead, polar-like PG
82 synthesis is redirected to mid-cell. These observations suggest that only FtsZ is required to
83 terminate polar growth and initiate cell division-specific PG biosynthesis at mid-cell, whereas
84 FtsZ, FtsA, and FtsW are exclusively required for cell division. Together these findings suggest
85 that *A. tumefaciens* uses sequential regulation of cell division, a theme that is broadly conserved
86 in bacteria.

87

88 **Results and Discussion**

89 **$FtsZ_{AT}$ is required for cell division and termination of polar growth.** *Agrobacterium*
90 *tumefaciens* contains three homologs of *Escherichia coli's* FtsZ, Atu_2086, Atu_4673, and
91 Atu_4215 (Figure 1A) [27]. *E. coli* FtsZ is comprised of three regions: the conserved N-terminal
92 tubulin-like GTPase domain, a C-terminal linker (CTL), and a conserved C-terminal peptide
93 (CTP), which anchors FtsZ to the membrane via interactions with FtsA [33]. Atu_2086 contains
94 each of these domains out of which the GTPase domain and CTP share 52% and 67% identity to
95 their respective domain in *E. coli* FtsZ, whereas the CTL is extended in length [27]. The gene
96 encoding Atu_2086 is found in a putative operon with genes encoding DdlB, FtsQ, FtsA [34, 35]
97 and is predicted to be essential for cell survival based on saturating transposon mutagenesis [36].
98 Atu_2086 localizes to mid-cell in wildtype (WT) pre-divisional cells (Figure 1B) [27, 29];
99 consistent with a role in cell division. Atu_4673 (called $FtsZ_1$; consistent with the genome

annotation) contains a complete GTPase domain with 49% identity to tubulin domain of *E. coli* FtsZ but lacks both the CTL and CTP [27]. Although Atu_4673 is not predicted to be required for cell survival based on saturating transposon mutagenesis [36], it localizes to mid-cell in pre-divisional cells, suggesting a possible role in cell division (Figure 1B). Atu_4215 (termed $FtsZ_3$ in this work) contains a partial GTPase domain with 48% identity to the N-terminal portion of the *E. coli* FtsZ tubulin domain and lacks both the CTL and CTP [27]. $FtsZ_3$ is not essential for survival of *A. tumefaciens* based on saturating transposon mutagenesis [36] and exhibits a diffuse localization pattern (Figure 1B). Together, these data suggest that Atu_2086 is the canonical FtsZ protein required for cell division, and this protein will be referred to as $FtsZ_{AT}$ throughout this work (although it is annotated as $FtsZ_2$ in the *A. tumefaciens* C58 genome [34, 35]).

To characterize the function of each FtsZ homolog, we constructed deletions of *ftsZ1* and *ftsZ3* and a depletion strain of *ftsZAT.* Since we were unable to construct a deletion of *ftsZAT,* we used a depletion strategy in which *ftsZAT* is present as a single copy under the control of an isopropyl β-D-1-thiogalactopyranoside (IPTG) inducible promoter at a neutral site in the chromosome [21, 32]. Using western blot analysis, we have confirmed the depletion of $FtsZ_{AT}$ in the absence of IPTG (Figure 1- Figure Supplement 1A).

Deletion of *ftsZ1* or *ftsZ3* does not impact cell viability (Figure 1C), cell morphology (Figure 1D; Table 1; Figure 1-Figure Supplement 1B), microcolony formation (Figure 1D), constriction rate or position (Table 1) when compared to WT cells. Similarly, when $FtsZ_{AT}$ is expressed in the depletion strain (labeled in Figures as $+FtsZ_{AT}$) the cells remain viable (Figure 1C), are similar in

size to WT cells (Table 1), properly position constrictions (Table 1), and form microcolonies (Figure 1D). In contrast, depletion of $FtsZ_{AT}$ (labeled in Figures as $–FtsZ_{AT}$) causes a marked decrease in cell viability (Figure 1C) and triggers the formation of large cells with complex branched morphologies (Table 1; Figure 1D). To quantify changes in morphology during depletion of $FtsZ_{AT}$, the cell area of at least 100 cells was calculated based on phase contrast images of cells acquired immediately after removal of the inducer ($-FtsZ_{AT}$ 0 h), 8 h after removal of the inducer ($-FtsZ_{AT}$ 8 h), and 14 h after removal of the inducer ($-FtsZ_{AT}$ 14 h) (Table 1, Figure 1- Figure Supplement 1C). Initially, the $FtsZ_{AT}$ depleted cells are similar to WT in cell size, but after 8 h of $FtsZ_{AT}$ depletion the cell area has nearly doubled (Table 1, Figure 1- Figure Supplement 1C). Within 14 h of $FtsZ_{AT}$ depletion, the average cell area has dramatically increased (Table 1, Figure 1- Figure Supplement 1C). Together, these results demonstrate that only the $FtsZ_{AT}$ homolog is required for proper cell growth and division.

		Average Cell Length[a] (μm +/- SD[b])	**Average Cell Area[a] (μm^2 +/- SD)**	**Average Constriction Rate[c] (nm/min +/- SD)**	**Relative Constriction Position[d] +/- SD**
WT		2.31 +/-.50	1.66 +/-.35	6.82 +/-3.19	.49 +/-.05
Δ*ftsZ*$_1$		2.25 +/-.49	1.52 +/-.33	6.99 +/-3.58	.46 +/-.05
Δ*ftsZ*$_3$		2.24 +/-.47	1.44 +/-.30	6.77 +/-2.77	.46 +/-.05
Δ*ftsZ*$_1$ Δ*ftsZ*$_3$		2.25 +/-.51	1.47 +/-.34	6.61 +/-3.75	.46 +/-.04
ftsZ$_{AT}$ depletion	- $FtsZ_{AT}$ 0 h	2.71 +/-.70	1.56 +/-.39	6.38 +/-2.81	.49 +/-.07
	- $FtsZ_{AT}$ 8 h	ND[e]	2.95 +/-1.12	ND	ND
	- $FtsZ_{AT}$ 14 h	ND	11.37 +/-4.69	ND	ND

Table 1. Quantitation of cell size and constriction of *ftsZ* mutants

[a]At least 100 cells were used to quantify the cell length and area for each strain

[b]SD – standard deviation.

[c]At least 30 cells were used to quantify the constriction rates for each strain

[d]Relative constriction position for at least 40 cells is shown. A value of 0 corresponds to the new pole, 0.5 corresponds to mid-cell, and a value of 1 corresponds to the old pole.

[e]ND – not determined.

Deletion of *ftsZ*$_1$ and *ftsZ*$_3$ does not change the FtsZ$_{AT}$ depletion phenotype. Since the *ftsZ*$_1$ and *ftsZ*$_3$ single deletions do not have an obvious impact on cell morphology, growth, or division, we constructed double and triple mutants to determine if there is an increasing effect when removing multiple *ftsZ* homologs. Double deletion of *ftsZ*$_1$ and *ftsZ*$_3$ does not cause a decrease in cell viability (Figure 2A, top panel), cell morphology (Table 1), or microcolony formation (Figure 2A, bottom panel). Furthermore, *ΔftsZ*$_1$ *ΔftsZ*$_3$ cells properly place constrictions and have an average constriction rate similar to WT (Table 1). Next, we introduced the *ΔftsZ*$_1$, *ΔftsZ*$_3$, and *ΔftsZ*$_1$ *ΔftsZ*$_3$ mutations into the *ftsZ*$_{AT}$ depletion strain to determine if loss of multiple *ftsZ* homologs further aggravated the *ftsZ*$_{AT}$ depletion phenotypes. The combination of the *ftsZ*$_{AT}$ depletion strain with *ΔftsZ*$_1$, *ΔftsZ*$_3$, or *ΔftsZ*$_1$ *ΔftsZ*$_3$ mutations did not result in a further decrease in cell viability (Figure 2B, top panel) or a worsening of cell morphology (Figure 2B, bottom panel) when compared to FtsZ$_{AT}$ depletion alone. Together, these results suggest that the FtsZ$_1$ and FtsZ$_3$ homologs do not have a major impact on cell division under the conditions tested.

ftsZ gene duplications have occurred independently in several alphaproteobacterial lineages and in chloroplasts and some mitochondria [37]. In most of the cases that have been studied, one

158 FtsZ homolog plays a canonical role in cell or organelle division while the other plays a
159 regulatory or specialized role. However, little is known about the roles of multiple ftsZs in
160 certain alphaproteobacteria species. In both *Rhizobium meliloti* and *Magnetospirillum*
161 *gryphiswaldense*, one of the FtsZs (containing a CTL and CTP similar to $FtsZ_{AT}$) is essential and
162 the other (truncated after the GTPase domain similar to $FtsZ_1$) is dispensable [38, 39]. In the case
163 of *M. gryphiswaldense*, the truncated *ftsZ* is dispensable for division but important for
164 biomineralization in this magnetotactic species under certain growth conditions. Similarly, it is
165 possible that $FtsZ_1$ or $FtsZ_3$ may have important contributions to cell growth or division of *A.*
166 *tumefaciens* in different environments as e.g. in its plant-associated life-style.

167

168 **$FtsZ_1$ requires $FtsZ_{AT}$ to localize to mid-cell and to polymerize *in vitro*.** Since $FtsZ_1$ localizes
169 to mid-cell (Figure 1B), we hypothesized that $FtsZ_1$ may be a nonessential divisome component.
170 To test this, we examined the localization of $FtsZ_1$-sfGFP in both WT and the *$ftsZ_{AT}$* depletion
171 strain (Figure 3). In WT and $FtsZ_{AT}$ induced cells, $FtsZ_1$-sfGFP does not localize in newborn
172 cells but forms FtsZ-like rings at the future site of division in pre-divisional cells (Figure 3A, top
173 and middle panel). This Z-like ring constricts to form a single focus in dividing cells. These
174 observations suggest that $FtsZ_1$ may be a divisome component despite the absence of a cell
175 division phenotype in the Δ*$ftsZ_1$* strain. To explore the possibility of interactions arising due to
176 the loss of $FtsZ_1$ and $FtsZ_{AT}$, we next visualized $FtsZ_1$-sfGFP localization during the depletion of
177 $FtsZ_{AT}$ (Figure 3A, bottom panel). We pre-depleted $FtsZ_{AT}$ for 4 h in liquid to avoid cell
178 crowding caused by division events prior to sufficient $FtsZ_{AT}$ depletion. Early during the
179 depletion of $FtsZ_{AT}$, $FtsZ_1$-sfGFP localizes in a FtsZ-like ring near mid-cell. However, as the

180 $FtsZ_{AT}$ depletion continues, $FtsZ_1$-sfGFP rings and foci progressively fade away, demonstrating
181 that localization of $FtsZ_1$-sfGFP to mid-cell requires the presence of $FtsZ_{AT}$.

182

183 Since $FtsZ_1$ is recruited to mid-cell by $FtsZ_{AT}$, we hypothesized that $FtsZ_{AT}$ and $FtsZ_1$ may form
184 co-polymers. To first test the ability of $FtsZ_{AT}$ and $FtsZ_1$ to independently form polymers, each
185 protein was purified and subjected to polymerization studies. Right angle light scattering assays
186 of wildtype $FtsZ_{AT}$ revealed that this protein exhibits a GTP-dependent increase in light
187 scattering at concentrations above 2 μm, consistent with its polymerization (Figure 3B, blue
188 lines). Negative stain transmission electron microscopy (TEM) confirmed that $FtsZ_{AT}$ forms
189 gently curved protofilaments in the presence of GTP (Figure 3C, left panel) and it rapidly
190 releases inorganic phosphate suggesting that GTP is hydrolyzed (Figure 3D, blue lines; 4.7 ± 0.2
191 GTP min^{-1} $FtsZ^{-1}$ at 8 μM $FtsZ_{AT}$, n=3). Surprisingly, we did not observe polymerization of
192 wildtype $FtsZ_1$, even at high protein concentrations either in light scattering (Figure 3B, red line),
193 TEM (Figure 3C, center panel), or GTP hydrolysis assays (Figure 3D, red line).

194

195 In light of the dependence of $FtsZ_1$ on $FtsZ_{AT}$ for mid-cell localization, we next sought to
196 determine if $FtsZ_{AT}$ and $FtsZ_1$ can form co-polymers. To conduct these experiments, $FtsZ_1$-
197 L71W and $FtsZ_{AT}$-L72W were purified to enable monitoring of protein polymerization using
198 tryptophan fluorescence. The leucine to tryptophan mutation introduces a tryptophan on the
199 surface of FtsZ that increases in fluorescence when it is buried in the subunit interface upon
200 polymerization [40]. While wildtype $FtsZ_{AT}$ (with no tryptophan) does not change in
201 fluorescence on addition of GTP (Figure 3E, solid blue line), $FtsZ_{AT}$-L72W fluorescence

202 increases rapidly after GTP addition reflecting polymerization (Figure 3E, dashed blue line).
203 When wildtype $FtsZ_{AT}$ is added to $FtsZ_{AT}$-L72W, bringing the total FtsZ concentration to 8 μM,
204 fluorescence again increases, but then drops back to baseline upon complete consumption of
205 GTP by this high concentration of FtsZ (Figure 3E, dotted blue line). Conversely, on its own or
206 combined with wildtype $FtsZ_1$, $FtsZ_1$-L71W maintains a constant tryptophan fluorescence level
207 before and after addition of GTP, consistent with our conclusion that it does not polymerize on
208 its own (Figure 3E, red lines). Remarkably, tryptophan fluorescence increases when $FtsZ_1$-L71W
209 and $FtsZ_{AT}$ are mixed, indicating that the $FtsZ_1$-L71W is incorporated into polymers in the
210 presence of $FtsZ_{AT}$ (Figure 3C, purple dashed line). When $FtsZ_{AT}$-L72W is mixed with $FtsZ_1$,
211 fluorescence increases above the level observed for $FtsZ_{AT}$-L72W alone and drops to baseline
212 faster than $FtsZ_{AT}$-L72W on its own, again indicating co-polymerization. Finally, equimolar
213 concentrations of $FtsZ_{AT}$ alone or mixtures of $FtsZ_{AT}$ and $FtsZ_1$ exhibit similar rates of GTP
214 hydrolysis (Figure 3D) and form qualitatively similar polymers by TEM (Figure 3C, right panel).
215 Together, these observations indicate that $FtsZ_1$ cannot polymerize independently, but that
216 $FtsZ_{AT}$ and $FtsZ_1$ form co-polymers with similar structure and GTP hydrolysis rates as $FtsZ_{AT}$
217 polymers.

218

219 Though multiple FtsZs are present in a number of bacterial and chloroplast lineages, their co-
220 assembly properties have only begun to be characterized. In contrast to our observations, each of
221 the FtsZs of *M. gryphiswaldense* was able to independently polymerize *in vitro*, but they also
222 appeared to directly interact, perhaps reflecting an ability to co-polymerize [39]. Chloroplast
223 FtsZs from *Arabadopsis thaliana* are also able to co-polymerize and, at least under some
224 conditions, to independently polymerize [41]. Conversely, one of the FtsZs from tobacco

chloroplasts cannot polymerize on its own but promotes polymerization of its partner homolog [42]. Finally, the FtsZ pair from the chloroplasts of representative green and red algae co-polymerize into polymers with altered assembly dynamics from either homopolymer [43]. It is likely that in each of these cases, the assembly or co-assembly properties of the duplicated FtsZs have evolved to suit a niche regulatory function. We hypothesize the $FtsZ_1$ from *A. tumefaciens* has low affinity for itself, but higher affinity for $FtsZ_{AT}$, limiting its homopolymerization but allowing for co-polymerization both *in vitro* and in cells. Since $FtsZ_1$ cannot polymerize independently, $FtsZ_{AT}$ must first polymerize at mid-cell after which $FtsZ_1$ can be recruited by co-polymerization. The biological relevance of these biochemical and cell biological properties awaits further study.

$FtsZ_{AT}$ depletion results in tip splitting events. Once we identified $FtsZ_{AT}$ as the primary homolog involved in cell division we next analyzed the growth phenotype during $FtsZ_{AT}$ depletion more carefully. Compared to $FtsZ_{AT}$ induced cells (Figure 4A, top), observation of cells during $FtsZ_{AT}$ depletion by time-lapse microscope reveals remarkable changes in cell morphology (Figure 4A, bottom; Movie 1). Early during the depletion of FtsZ, an ectopic pole forms near mid-cell. We hypothesize that this occurs due to the ability of the remaining FtsZ to identify the mid-cell and recruit PG biosynthesis machinery to that site. Both the original growth pole and the ectopic pole are growth-active, resulting in the presence of multiple growth poles. These growth poles are unable to terminate cell elongation and ultimately most growth active poles are split, leading to the accumulation of many growth active poles (Figure 4A, bottom; Movie 1) and the rapid increase in cell area until the cell lyses.

The branched morphology observed during $FtsZ_{AT}$ depletion is in stark contrast to FtsZ depletion observed in other organisms. In species like *E. coli* and *B. subtilis*, which utilize laterally localized peptidoglycan biosynthesis during elongation, depletion of FtsZ results in long, smooth filamentous cells. We hypothesize that the branching morphology of the *A. tumefaciens* $FtsZ_{AT}$ depletion strain can be attributed to polar elongation. During the block in cell division, the growth pole continues to grow and presumably recruits additional peptidoglycan biosynthesis proteins. This could lead to an over-accumulation of elongasome proteins causing the pole to split into two poles. A similar branching pattern has been characterized during typical growth of *Streptomyces coelicolor* [44]. In this polar growing bacterium, the established elongasome splits, leaving a small portion of the elongasome behind as growth continues. With time, the subpolar elongasome accumulates in size and eventually forms a new growth pole. Although the polar growth molecular mechanisms are not conserved between *A. tumefaciens* and *S. coelicolor*, the fundamental principle of tip splitting as a consequence of polar growth appears to be shared.

PopZ-YFP accumulates at growth poles in the absence of $FtsZ_{AT}$. In WT *A. tumefaciens*, deletion of *popZ* has been shown to cause ectopic poles and cells devoid of DNA, demonstrating a role in coordinating cell division with chromosome segregation [45, 46]. We hypothesize that PopZ-dependent coordination of cell division likely involves FtsZ. In WT, PopZ-YFP localizes to the growing pole during elongation and is recruited to mid-cell just prior to cell separation (Figure 4B, top panel) [45-47]. When $FtsZ_{AT}$ is expressed in the *ftsZ$_{AT}$* depletion strain, PopZ-YFP has a similar localization pattern as in WT cells (Figure 4B, middle panel). When $FtsZ_{AT}$ is depleted, PopZ-YFP stays at the growth poles and as tip splitting events lead to the production of new growth poles, PopZ-YFP appears to be split and retained at all growth active poles (Figure

4B, bottom panel). These observations indicate that FtsZ is required for mobilizing PopZ from the growth pole to mid-cell. Remarkably, both FtsZ and FtsA are mislocalized in the absence of PopZ, leading to the establishment of asymmetric constrictions sites and a broad range of cell lengths [45]. Together, these data suggest that the presence of both PopZ and FtsZ are important for proper positioning and functioning of the divisome.

In addition to its function in maintaining proper cell division, *A. tumefaciens* PopZ is also required for chromosome segregation and tethers the centromere of at least one chromosome to the growth pole [46]. Thus, we examined the DNA content of cells depleted of $FtsZ_{AT}$. In both WT cells and in conditions where $ftsZ_{AT}$ is induced in the $ftsZ_{AT}$ depletion strain, DNA labeled with Sytox orange is diffuse throughout most cells (Figure 4C, top two panels). In late divisional cells, true separation of nucleoids is observed indicating successful completion of chromosome segregation (Figure 4C, marked with an asterisk in the top two panels). In cells depleted of $FtsZ_{AT}$ for both 8 and 14 h, DNA is diffuse throughout the elongated branches (Figure 4C, bottom two panels). The absence of distinct nucleoids may suggest that final stages of chromosome segregation are coordinated with cell separation as has been described for other bacteria including *E. coli* and *C. crescentus* [48].

To look more carefully at genomic content, we visualized YFP-ParB1, which serves as a proxy to track centromere partitioning in *A. tumefaciens* [46], in WT and $ftsZ_{AT}$ depletion cells. In both WT cells and cells expressing $FtsZ_{AT}$ in the $ftsZ_{AT}$ depletion strain, a single YFP-ParB1 focus is present at the old pole in new cells generated by a recent cell division event (Figure 4D, top and

middle panels). As the cells elongate, a second focus appears and translocates across the longitudinal axis to the growing pole (Figure 4D, top and middle panels). After 4 h of $FtsZ_{AT}$ pre-depletion, YFP-ParB1 foci can be seen at both poles, but when the cell fails to divide, a third focus of YFP-ParB1 appears and translocates along the longitudinal axis of the cell before taking a rapid turn toward a new ectopic pole formed from near mid-cell (Figure 4D, bottom panel). Next, we quantified the number of YFP-ParB1 foci relative to cell area (Figure 4E). In WT and $FtsZ_{AT}$ expressing cells in the *ftsZ*$_{AT}$ depletion strain, small cells have only a single focus of YFP-ParB1. This is followed by a transition period in which elongating cells accumulate a second focus of YFP-ParB1. Finally, the largest, pre-divisional cells have two YFP-ParB1 foci (Figure 4E). Cells depleted of $FtsZ_{AT}$ for 8 h accumulate YFP-ParB1 foci as they increase in area (Figure 4E). Cells with an area larger than 3 μm^2 all have at least 2 YFP-ParB1 foci, suggesting that chromosome replication is not blocked during FtsZ depletion. Furthermore, in larger cells additional YPF-ParB1 foci accumulate. These data suggest that cell division is not strictly required for the initiation of DNA replication in *A. tumefaciens*, although completion of chromosome segregation may be coordinated with cell division.

Loss of septal PG synthesis results in altered total PG composition. Since polar growth appears to continue in the absence of FtsZ (Figure 4A, bottom panel), we used fluorescent-D-amino acids (FDAAs), to probe sites enriched in peptidoglycan synthesis [49] during depletion of $FtsZ_{AT}$. In WT cells, FDAAs localize at a single pole in elongating cells and at mid-cell in pre-divisional cells (Figure 5A) [49]. As $FtsZ_{AT}$ is depleted, FDAAs are targeted strictly to the poles, confirming that polar peptidoglycan synthesis is responsible for the observed increase in cell biomass after 8 h and 14 h of depletion (Figure 5A).

316

317 Since cells depleted of $FtsZ_{AT}$ fail to terminate polar growth and do not produce septal
318 peptidoglycan, we hypothesized that the peptidoglycan composition may reveal chemical
319 signatures of peptidoglycan derived from polar growth. Thus, we characterized the
320 peptidoglycan composition of both WT cells and the *ftsZ*$_{AT}$ depletion strain in both the presence
321 and absence of IPTG using ultra-performance liquid chromatography (UPLC) [50]. The major
322 muropeptides found in WT *A. tumefaciens* PG and their quantification are shown in (Figure 5-
323 Figure Supplement 1) and include monomeric (M), dimeric (D), and trimeric (T) muropeptides.
324 The muropeptide composition and abundance is similar between WT cells, WT cells grown in
325 the presence of IPTG, and the *ftsZ*$_{AT}$ depletion strain grown in the presence of IPTG such that
326 $FtsZ_{AT}$ is expressed (Figure 5- Figure Supplement 1). These findings suggest that there are no
327 major changes in PG composition due to IPTG and that the presence of IPTG leads to
328 complementation in the *ftsZ*$_{AT}$ depletion strain. In contrast, when the *ftsZ*$_{AT}$ depletion strain is
329 grown in the absence of IPTG for 14 h, marked changes in muropeptide composition are
330 observed (Figure 5B-D). While the overall abundance of monomeric, dimeric, and trimeric
331 muropeptides are not dramatically impacted (Figure 5C), the abundance of specific muropeptides
332 is modified. When $FtsZ_{AT}$ is depleted, there is a significant increase in monomeric disaccharide
333 tripeptide (M3) and a decrease in the abundance of the monomeric disaccharide tetrapeptide M4
334 (Figure 5B). This observation is consistent with the possibility that the absence of $FtsZ_{AT}$ leads to
335 an increase in LD-carboxypeptidase activity, which would remove the terminal peptide from M4,
336 leading to both a reduction in the levels of M4 and an increase in the abundance in M3.
337 Following $FtsZ_{AT}$ depletion, the overall degree of muropeptide crosslinking decreases (Figure
338 5D). In particular, there is a marked decrease in DD-crosslinkages, which are formed by the DD-

transpeptidase activity associated with penicillin-binding proteins (PBPs). The dominant dimeric muropeptide formed in the presence of $FtsZ_{AT}$ is D44, which contains a DD-crosslink; in contrast, the dominant dimer formed in the absence of $FtsZ_{AT}$ is D33, which contains an LD-crosslink (Figure 5B). These data suggest that the activity of LD-transpeptidases is increased and the activity of PBP-mediated DD-transpeptidases is decreased during $FtsZ_{AT}$ depletion. The increased pool of M3 may provide additional acceptor substrate for LD-transpeptidases to increase the production of D33 relative to D44. In addition, increased LD-carboxypeptidase activity could contribute to increase further the levels of D33 using D34 as a substrate.

The *A. tumefaciens* genome contains 14 LD-transpeptidases, 7 of which are specific to Rhizobiales. The Rhizobiales-specific LD-transpeptidase encoded by *Atu_0845* (referred to here as $LDTP_{0845}$) has been shown to localize to the growing pole in WT cells and has been hypothesized to contribute to polar growth [30]. This localization pattern was confirmed in both WT and $FtsZ_{AT}$ induced cells (Figure 5E, top and middle panels). We find that $LDTP_{0845}$ localizes at growth poles during depletion of $FtsZ_{AT}$ (Figure 5E, bottom). This observation suggests that this $LDTP_{0845}$ may contribute to changes in PG composition during $FtsZ_{AT}$ depletion and supports a potential role for LD-transpeptidases in polar growth during elongation. The localization and function of putative periplasmic LD-carboxypeptidases in *A. tumefaciens* remain to be explored. Overall, these findings suggest that LD-carboxypeptidase and LD-transpeptidase activities are increased during $FtsZ_{AT}$ depletion, indicating that these classes of enzymes may contribute to polar growth of *A. tumefaciens*.

The C-terminal Conserved Peptide (CTP) of $FtsZ_{AT}$ is required for proper termination of polar growth. To better understand the mechanism by which $FtsZ_{AT}$ terminates polar growth, we constructed truncated proteins to analyze the function of the C-terminal conserved peptide (CTP) and the C-terminal linker (CTL) (Figure 1A). The CTP is a highly conserved domain which binds to proteins such as FtsA, that tether FtsZ to the membrane [37, 51, 52]. The CTL is an intrinsically disordered region of variable length found in FtsZ proteins, which functions in the regulation of PG biosynthesis and protofilament assembly [17, 53-55]. To probe the function of the $FtsZ_{AT}$ CTP and CTL domains, we expressed $FtsZ_{AT}$ΔCTP and $FtsZ_{AT}$ΔCTL in both WT and $FtsZ_{AT}$ depletion backgrounds.

In order to execute these experiments, we constructed a vector with an alternative "inducible" promoter system, which is compatible with the chromosomal IPTG depletion system. We modified pSRKKm [56] by replacing *lacI*^{q} with the gene encoding the cumate responsive repressor CymR [57, 58] and replacing the *lacO* operator sites with *cuO* operator sites (Figure 6-Figure Supplement 1A). This approach allows the same promoter to drive expression of both chromosomal full-length *ftsZ*$_{AT}$ using IPTG and plasmid-encoded *ftsZ* variants using cumate. For simplicity, henceforth we referred to IPTG induction as mediated by P_{lac} and cumate induction as mediated by P_{cym}. Expression of sfGFP from P_{cym} requires the presence of cumate (Figure 6-Figure Supplement 1B) and is comparable to expression of sfGFP from P_{lac} (Figure 6- Figure Supplement 1C). Although higher concentrations of cumate inhibit growth of WT *A. tumefaciens*, 0.01 mM cumate does not impair growth of WT cells (Figure 6- Figure Supplement 1D; left) and is sufficient to complement growth of the *ftsZ*$_{AT}$ depletion strain in the absence of IPTG (Figure 6- Figure Supplement 1D; right).

384

385 In the *ftsZ$_{AT}$* depletion strain, we introduced 4 vectors: an empty vector with P$_{cym}$ (pEmpty), P$_{cym}$-
386 *ftsZ$_{AT}$* (pFtsZ$_{AT}$), P$_{cym}$-*ftsZ$_{AT}$*Δ*CTP* (pFtsZ$_{ΔCTP}$) or P$_{cym}$-*ftsZ$_{AT}$*Δ*CTL* (pFtsZ$_{ΔCTL}$). When full-length
387 *ftsZ$_{AT}$* is expressed from the chromosome, the viability of cells is not impacted by the presence of
388 the P$_{cym}$ vectors (Figure 6A, top left panel). In the absence of induction of *ftsZ* from the
389 chromosome, the presence of the uninduced P$_{cym}$ vectors, including pFtsZ$_{AT}$, is not sufficient to
390 rescue viability of the FtsZ-depleted cells (Figure 6A, top right panel); however, viability is
391 significantly restored by expression of plasmid-encoded FtsZ$_{AT}$ in the presence of cumate
392 (Figure 6A, bottom left panel). Expression of plasmid-encoded FtsZ$_{AT}$ΔCTP partially rescues the
393 depletion of FtsZ$_{AT}$ (Figure 6A, bottom left panel). In contrast, expression of plasmid-encoded
394 FtsZ$_{AT}$ΔCTL does not rescue the depletion of FtsZ$_{AT}$ (Figure 6A, bottom left panel) and when
395 both chromosomal full-length FtsZ$_{AT}$ and FtsZ$_{AT}$ΔCTL are expressed, viability is impaired,
396 suggesting that FtsZ$_{AT}$ΔCTL may have a dominant negative phenotype (Figure 6A, bottom right
397 panel).

398

399 Next, we observed cell morphology of the *ftsZ$_{AT}$* depletion strain carrying each of the four
400 vectors under conditions where the chromosomal FtsZ$_{AT}$ is depleted and the plasmid-encoded
401 FtsZ variants are expressed for 6 or 14 h (Figure 6B). The presence of pEmpty does not impact
402 the FtsZ$_{AT}$ depletion phenotype: branched cells with multiple growth active poles are observed
403 (Figure 6B). Plasmid-encoded FtsZ$_{AT}$ rescues the chromosomal FtsZ$_{AT}$ depletion, resulting in the
404 production of typical rod-shaped cells with PG biosynthesis occurring at a single pole or mid-cell
405 (Figure 6B, middle left). The partial rescue of FtsZ$_{AT}$ depletion in viability by expression of
406 FtsZ$_{AT}$ΔCTP was matched by a less severe defect in cell morphology (Figure 6B, middle right).

Although cells are branched, they are much shorter and have fewer branches than $FtsZ_{AT}$ depletion. FDAA labeling reveals that the expression of $FtsZ_{AT}$ΔCTP enables mid-cell labeling (Figure 6B, middle left), suggesting that PG is synthesized at mid-cell and that some cells may undergo division. Indeed, time-lapse microscopy of the $FtsZ_{AT}$ depletion strain expressing only FtsZΔCTP reveals that the cells are capable of cell division events (Figure 6C, top panel). Remarkably, the sites of cell constriction and cell division are often asymmetric, giving rise to a cell population with a broad length distribution. Furthermore, polar growth is not terminated efficiently and both polar elongation and tip splitting events are evident. Together, these observations suggest that the FtsZ CTP contributes to proper termination of polar growth and divisome assembly. Expression of plasmid-encoded $FtsZ_{AT}$ΔCTL in the absence of chromosome-encoded $FtsZ_{AT}$ gives rise to a distinct cell morphology (Figure 6B, far right panel). After 6 hours of $FtsZ_{AT}$ΔCTL expression, some cells contain mid-cell bulges. Remarkably, in these cells, FDAA labeling reveals that PG biosynthesis is occurring in the bulges and not at either pole. After 14 h, most cells have mid-cell swelling and multiple ectopic poles. Time-lapse microscopy reveals that polar growth is terminated and growth appears to be directed to mid-cell (Figure 6C, bottom panel, 320 min). When cell division fails, ectopic growth poles emerge from the mid-cell bulges (Figure 6C, bottom panel 520 min). The ectopic poles elongate, polar growth is terminated, and new ectopic growth poles are formed near the initial bulge site (Figure 6C, bottom panel). These observations suggest that the CTL of $FtsZ_{AT}$ is required for proper cell division but is not required for the termination of polar growth.

The CTL of $FtsZ_{AT}$ is required for proper PG composition. The mid-cell bulges observed during FtsZΔCTL expression are reminiscent of those observed when $FtsZ_{CC}$ΔCTL is expressed

in *C. crescentus* [17]. In *C. crescentus*, the CTL was shown to be required for robust PG biosynthesis [17]. We therefore hypothesized that the altered PG composition observed during depletion of $FtsZ_{AT}$ could be due to absence of the CTL. To test this hypothesis, we introduced plasmids containing no FtsZ (empty vector control, pEmpty), full-length $FtsZ_{AT}$ ($pFtsZ_{AT}$), or $FtsZ_{AT}\Delta CTL$ ($pFtsZ_{AT}\Delta CTL$) into the *ftsZ* depletion strain. Each strain was grown under conditions in which expression of $FtsZ_{AT}$ from the chromosomal copy is depleted and expression of the FtsZ variant (if present) from the plasmid is induced. PG was isolated from these strains following induction/depletion and analyzed. Induction of full-length $FtsZ_{AT}$ from the plasmid yields lower levels of monomeric muropeptides compared to other strains, especially M3, and increased levels of dimeric and trimeric muropeptides, including D44 and T444 (Figure 7A-B). Overall the expression of full-length $FtsZ_{AT}$ leads to an increased level of muropeptides with DD-crosslinks (Figure 7C). These observations indicate that expression of plasmid-encoded full-length $FtsZ_{AT}$ compensates for the loss of $FtsZ_{AT}$ from the chromosome. In contrast, the expression of $FtsZ_{AT}\Delta CTL$ did not compensate for the loss of full-length FtsZ as the PG composition is more similar to the PG profile of FtsZ-depleted cells (Figure 7A-C). This observation suggests that the CTL of $FtsZ_{AT}$ likely function in the regulation of proper PG biosynthesis at mid-cell.

FtsZ CTL regulates protofilament assembly. Work in *C. crescentus* has shown that the $FtsZ_{CC}$CTL directly regulates protofilament structure and dynamics [53]. To determine if the CTL of $FtsZ_{AT}$ similarly regulates its assembly, we purified $FtsZ_{AT}\Delta CTL$ and a control $FtsZ_{AT}$+CTL protein containing the same restriction sites at the junctions with the GTPase domain and CTP as the ΔCTL construct, but with the CTL in place. $FtsZ_{AT}$+CTL formed mostly

453 single, gently curved protofilaments when visualized by TEM under all conditions tested (Figure
454 7D), similar to those observed for wildtype $FtsZ_{AT}$ (Figure 3C). In contrast, under high salt
455 conditions we observed extended bundles of $FtsZ_{AT}\Delta CTL$ (Figure 7D). Furthermore, we saw a
456 decreased rate of GTP hydrolysis by $FtsZ_{AT}\Delta CTL$ under conditions that promote bundling
457 (Figure 7D; 3.3 ± 0.2 GTP min^{-1} $FtsZ^{-1}$ for $FtsZ_{AT}$+CTL and 2.1 ± 0.1 GTP min^{-1} $FtsZ^{-1}$ for
458 $FtsZ_{AT}\Delta CTL$ with 300 mM KCl, n =3). Together, these results suggest an important role for the
459 CTL in limiting lateral interactions between protofilaments and promoting polymer turnover.
460 These results in *A. tumefaciens* are consistent with effects of the CTL on polymer bundling
461 reported in *C. crescentus* [17, 53]and *E. coli* [59]. Moreover, in light of our observations that
462 $FtsZ_{AT}\Delta CTL$ does not restore proper PG chemistry to $FtsZ_{AT}$-depleted cells (Figure 7A,B), these
463 data are in line with the growing body of evidence linking FtsZ dynamics and polymer
464 superstructure to the regulation of PG biosynthesis.

465

466 **FtsA is required for cell division but not termination of polar growth.** FtsA is an actin-like
467 protein that associates with the membrane through an amphipathic helix and binds the FtsZ CTP
468 to anchor FtsZ polymers to the membrane [51, 60]. In *C. crescentus*, recruitment of FtsA to mid-
469 cell occurs well after the establishment of the FtsZ-ring and is dependent on the presence of FtsZ
470 [13, 61]. In *A. tumefaciens*, FtsA-sfGFP is retained at the growth pole prior to appearing at mid-
471 cell just before cell division [27, 30]. Here, we confirm that FtsA-sfGFP is observed as a focus at
472 the growth pole until transitioning to a ring-like structure at mid-cell (Figure 8A, top panelIn
473 fact, at some timepoints, both a polar focus and a mid-cell ring of FtsA are observed. Eventually,
474 the polar focus disappears as the FtsA-sfGFP ring becomes more intense just prior to cell
475 division. During the depletion of $FtsZ_{AT}$, a focus of FtsA-sfGFP can be found at the growing

476 pole, and at a newly formed ectopic pole near mid-cell (Figure 8A, bottom panel). FtsA-sfGFP
477 remains associated with each growth pole, and as the poles undergo tip splitting events, each
478 focus of FtsA-sfGFP is also split, resulting in the presence of FtsA-sfGFP in each of the 4
479 growth-active poles. These observations suggest that $FtsZ_{AT}$ is required not only for proper mid-
480 cell localization of FtsA to mid-cell prior to cell division but also contributes to release of FtsA-
481 sfGFP from the growth pole.

482 Since FtsA tethers FtsZ to the membrane and enables divisome assembly [37, 51, 52] in *E. coli*,
483 we expected that the depletion of FtsA would phenocopy the depletion of FtsZ. Although a
484 saturating transposon mutagenesis screen indicated that *ftsA* is not essential for *A. tumefaciens*
485 cell survival [36], we were unable to construct a Δ*ftsA* mutant. Thus, we constructed a depletion
486 strain in which expression of *ftsA* is controlled by P_{lac}. Under conditions where FtsA is present in
487 the *ftsA* depletion strain, cells maintain proper rod-shaped morphology, polar growth, and cell
488 division occurs from constrictions formed near mid-cell (Figure 8B-C, top panels). In contrast,
489 when FtsA is depleted, cells exhibit a marked change in morphology (Figure 8B, bottom panel;
490 Movie 2). During the depletion of FtsA, rod-shaped cells initially elongate from a growth pole
491 (Figure 8B, bottom panel, 0 min). Polar growth is terminated and growth is re-initiated from near
492 mid-cell, typically resulting in the formation of two ectopic poles perpendicular to the original
493 longitudinal axis of the cell (Figure 8B, bottom panel, 170 min). Cells depleted of FtsA continue
494 multipolar growth (Figure 8B, bottom panel, 360 min), terminate growth from both poles and
495 reinitiate growth from near mid-cell resulting in the formation of a new pair of ectopic growth
496 poles (Figure 8B, bottom panel, 510 min). This pattern of multipolar growth, polar growth
497 termination, and new branch formation is continued until cells eventually bulge at the mid-cell
498 and lyse. Overall these observations indicate that the phenotypes caused by FtsZ and FtsA

499 depletion are distinct from one another and suggest that only FtsZ is required for proper
500 termination of polar growth.

501

502 To confirm that polar growth occurs and is terminated during FtsA depletion, cells were labeled
503 with FDAAs (Figure 8C, bottom panel). Indeed, FDAAs label the tips of two poles, which are
504 emerging from near mid-cell consistent with the re-initiation of polar growth. To further confirm
505 that polar growth is terminated during FtsA depletion, we observed the localization of PopZ-YFP
506 (Figure 8D, top panel). PopZ marks the growth poles [47] and becomes trapped at growth poles
507 during depletion of FtsZ (Figure 4B). During FtsA depletion, PopZ-YFP is initially present at the
508 growth pole (Figure 8D, top panel, 0 min). Next, PopZ-YFP disappears from the growth poles
509 and reappears near mid-cell (Figure 8D, top panel, 80 min) indicating that polar growth is
510 terminated. Throughout the FtsA depletion, PopZ-YFP continues to disappear from growth poles
511 and reappears at the tips of newly emerging growth poles. Overall, these observations clearly
512 indicate that FtsA is not necessary for termination of polar growth; however, FtsA has an
513 essential function at a later stage of cell division since the cells fail to divide and are prone to
514 lysis.

515

516 The ability of cells to target growth to near mid-cell during FtsA depletion suggests that FtsZ-
517 rings may form, enabling the termination of polar growth. Indeed, $FtsZ_{AT}$-sfGFP-rings form near
518 mid-cell early during FtsA depletion (Figure 8D, bottom panel). $FtsZ_{AT}$-sfGFP is briefly retained
519 at new growth poles before reappearing to mark the site where a new growth pole will emerge.
520 These observations are consistent with the finding the FtsA is retained at the growth pole longer

than FtsZ [27, 62], and suggest that FtsA arrives at mid-cell after Z-ring assembly and the initiation of FtsZ-dependent cell wall biogenesis. The results observed here in *A. tumefaciens* are consistent with the observation that FtsA arrives to mid-cell after FtsZ and the onset of mid-cell cell wall biogenesis in *C. crescentus* [13, 61]. In both *A. tumefaciens* and *C. crescentus*, the late arrival of FtsA to the divisome suggests that other proteins contribute to proper tethering of FtsZ to the membrane. In *C. crescentus*, the FtsZ-binding protein, FzlC, functions as a membrane anchor early during the establishment of the divisome [31, 63]. A homolog of FzlC is readily found in the *A. tumefaciens* genome (Atu2824) and may contribute to the ability of FtsZ-rings to form in the absence of FtsA.

Depletion of the downstream divisome component FtsW phenocopies depletion of FtsA. Having observed a distinct effect on cell morphology in the absence of *ftsA*, we wondered if the phenotype observed during *ftsA* depletion could be recapitulated in the absence of another late-arriving divisome protein. To test this hypothesis, we constructed a depletion strain of FtsW, which is recruited to mid-cell after FtsA in both *E. coli* and *C. crescentus* divisome assembly models [11, 13]. Depletion of FtsW results in a phenotype which is strikingly similar to the depletion of FtsA (Figure 9). When FtsW is induced normal growth is observed (Figure 9A, top panel). During FtsW depletion, polar growth is terminated, resulting in the establishment of growth-active poles from near mid-cell (Figure 9A, bottom panel; Movie 3). Multiple rounds of termination of polar growth followed by reinitiation of growth from near mid-cell occur until the mid-cell bulges and the cells ultimately lyse (Figure 9A, bottom panel). Labeling of growth active poles with FDAAs (Figure 9B) or by tracking PopZ-YFP localization (Figure 9C, top panel) confirmed that new branches which emerge from mid-cell are formed by polar growth.

Finally, we confirmed that FtsZ-rings form during the depletion of FtsW and the presence of an $FtsZ_{AT}$-sfGFP-ring typically marks the site where an ectopic growth pole will form (Figure 9C, bottom panel). Together, these observations suggest that FtsZ-rings are formed in the absence of FtsW, enabling the initiation of cell wall biogenesis. Given that FtsW drives septal PG biosynthesis, [64] these findings indicate that the cell wall biogenesis that occurs during depletion of FtsA or FtsW may require the elongation machinery, which typically functions in polar growth. Since the elongation machinery for *A. tumefaciens* remains to be identified, it is possible that there is considerable overlap between the machineries that contribute to polar and septal PG biosynthesis.

Concluding Remarks

While many questions remain unanswered about the regulation of cell wall biogenesis in *A. tumefaciens*, our work sheds light on the transition from polar growth to mid-cell growth. We find that $FtsZ_{AT}$, FtsA, and FtsW are required for constriction and cell separation, but $FtsZ_{AT}$ is also required to terminate polar growth and initiate mid-cell peptidoglycan synthesis. How might the formation of an $FtsZ_{AT}$-ring at mid-cell cause the termination of polar growth? We find that PopZ, and $LDTP_{0845}$ become trapped at the growth poles during FtsZ depletion (Figure 5). It is possible that one or more of these proteins contributes to both polar peptidoglycan biosynthesis and mid-cell peptidoglycan synthesis and that the FtsZ-dependent targeting of these proteins (and likely others) to mid-cell triggers the termination of polar growth. While the mid-cell localization of PopZ is dependent on the presence of $FtsZ_{AT}$ (Figure 4), $FtsZ_{AT}$-ring stability and placement are impacted by the absence of PopZ [45]. Furthermore, deletion of *popZ* impairs termination of polar growth and results in cell division defects [45, 46, 65]. The apparent co-dependence of FtsZ and PopZ for localization may suggest that these proteins function together during the early

568 stages of cell division, particularly the termination of polar growth and onset of mid-cell PG
569 biosynthesis.

570

571 Overall, our results are consistent with a general model, which is highly conserved in bacteria, in
572 which the establishment of a FtsZ-ring leads to the recruitment of many other cell division
573 proteins to mid-cell [11], though many mechanistic questions remain. How is $FtsZ_{AT}$ targeted to
574 mid-cell? A variety of mechanisms that contribute to the proper placement of FtsZ at mid-cell
575 have been described (for review see [66, 67]). The most well studied mechanisms of FtsZ
576 positioning include negative regulation by the Min system and nucleoid occlusion. While genes
577 encoding components of the Min system are readily identifiable in the *A. tumefaciens* genome,
578 the deletion of *minCDE* has a minimal impact on placement of constriction sites and cell division
579 efficiency [68]. Furthermore, $FtsZ_{AT}$-GFP rings form over DNA prior to nucleoid separation in
580 *A. tumefaciens*. These observations indicate that additional regulatory mechanisms must
581 contribute to proper division site selection in *A. tumefaciens*. Following the appearance of FtsZ at
582 mid-cell, how is the $FtsZ_{AT}$-ring stabilized? In *E. coli*, the FtsZ-ring is stabilized by interactions
583 with FtsA and ZipA, which tether FtsZ filaments to the membrane [51, 52, 69, 70]. In *A.*
584 *tumefaciens*, $FtsZ_{AT}$ appears at mid-cell well before FtsA [30] and we observe that $FtsZ_{AT}$ rings
585 form even when FtsA is depleted (Figure 7C, bottom panel). Furthermore, the position of
586 $FtsZ_{AT}$-GFP rings marks the site of ectopic pole formation. These observations suggest the
587 $FtsZ_{AT}$ is stabilized, at least early during cell division by other proteins. While there are no
588 obvious ZipA homologs encoded in the *A. tumefaciens* genome, a homolog of FzlC, which
589 functions to stabilize FtsZ in *C. crescentus* [31, 63], is encoded in the genome.

590

591 The observation that FtsZ is necessary for the initiation of mid-cell PG biosynthesis suggests that
592 FtsZ is necessary for recruitment of PG biosynthesis enzymes to mid-cell. Septal PG
593 biosynthesis is likely mediated by FtsW, a putative PG glycosyltransferase [71-73], and PBP3
594 (FtsI), a PG DD-transpeptidase [74]. In *A. tumefaciens*, depletion of FtsW does not cause a
595 complete block of PG synthesis at mid-cell (Figure 8). This observation suggests that mid-cell
596 PG biosynthesis is mediated by other cell wall biogenesis enzymes while the activity of FtsW
597 contributes to later stages of cell division, consistent with the inability of cells to form
598 constrictions and separate in the absence of FtsW. These observations may indicate that the
599 initial PG biosynthesis at mid-cell comprises the final stage of cell elongation, consistent with
600 descriptions of FtsZ-dependent mid-cell elongation in *C. crescentus* [16]. The observation that
601 growth-active, ectopic poles emerge from near mid-cell during FtsW depletion (Figure 8B)
602 provides evidence in support of this possibility. Thus, FtsZ-dependent PG biosynthesis may
603 contribute to both elongation and cell division in *A. tumefaciens*. For a polar growing bacterium,
604 it is tempting to speculate that the retention of PG biosynthesis machinery dedicated to
605 elongation at the site of cell division may prime the newly formed poles to become growth active
606 following cell separation.

607

608 **Materials and Methods**

609 **Bacterial strains and culture conditions.** All bacterial strains and plasmids used are listed in
610 Table S4.1. *A. tumefaciens* strains were grown in ATGN minimal medium with .5% glucose [75]
611 at 28°C. *E. coli* strains were grown in Luria-Bertani medium at 37°C. When indicated,
612 kanamycin (KM) was used at 300 µg/ml for *A. tumefaciens*, 50 µg/ml for *E. coli* DH5α, and 25
613 µg/ml for *E. coli* S17-1 λ *pir*. Gentamicin was used when indicated at 200 µg/ml for *A.*

614 *tumefaciens* and 20 μg/ml for *E. coli* DH5α. IPTG was added at a concentration of 1 mM when
615 indicated. Cumate was added at a concentration of 0.1 mM when indicated.

616

617 **Construction of expression plasmids and strains.** All strains and plasmids used are listed in
618 Table S4.1, while primers used are listed in Table S4.2. For amplification of target genes, primer
619 names indicate the primer orientation and added restriction sites. To construct expression vectors
620 containing *ftsZ*$_{AT}$-*sfgfp*, *ftsZ*$_{1}$-*sfgfp*, *ftsZ*$_{3}$-*sfgfp*, and *ldtp*$_{0845}$-*sfgfp* the respective coding sequence
621 was amplified from purified C58 genomic DNA using primers indicated in Table S4.2. The
622 amplicons were digested overnight and ligated into cut pSRKKM-P$_{lac}$-*sfgfp* using NEB T4 DNA
623 ligase at 4°C overnight. The newly formed *sfgfp* fusion of each gene was excised from the
624 plasmid by overnight digestion with NdeI and NheI. Fragments containing *ftsZ*$_{AT}$-*sfgfp*, *ftsZ*$_{1}$-
625 *sfgfp*, *ftsZ*$_{3}$-*sfgfp*, and *ldtp*$_{0845}$-*sfgfp* were then ligated into cut pRV-MCS2 to give constitutive
626 expression vectors containing the fusions. To construct the *popZ-yfp* expression vector, *popZ*
627 along with the upstream promoter sequence were amplified from purified C58 genomic DNA,
628 digested and ligated into pMR10.

629

630 To construct pSRKKM-P$_{cym}$, a synthesized gBlock from IDT Integrated DNA Technologies was
631 made containing the regulatory elements of the cumate system similar to previously described
632 plasmid constructs [76, 77]. The P$_{cym}$ promoter region is annotated in Table S4.2. The sequence
633 encoding the cumate repressor was codon optimized for *A. tumefaciens* and placed under the
634 control of the constitutive kanamycin promoter from pSRKKm-P$_{lac}$-sf*gfp*. The synthesized
635 gBlock was digested overnight with EcoRI and NdeI. The resulting fragment was then ligated

636 into cut pSRKKm-P_{lac}-sf*gfp* thereby replacing the original *lac* promoter and repressor with the
637 cumate repressor and cumate regulated promoter.

638

639 Next, *yfp-parB* was excised from pSRKKM-P_{lac}-*yfp-parB* [46] and ligated into pSRKKM-P_{cym} to
640 create an expression vector compatible with the depletion strains. To create expression vectors
641 for $ftsZ_{AT}$, $ftsZ_{AT}\Delta CTP$, and $ftsZ_{AT}\Delta CTL$ the respective target gene was amplified utilizing
642 indicated primers, digested overnight with NdeI and BamHI and ligated into pSRKKM-P_{cym}.

643 All expression vectors were verified by sequencing. All vectors were introduced into *A.*
644 *tumefaciens* strains utilizing standard electroporation protocols [78] with the addition of IPTG in
645 the media when introducing plasmids into in depletion backgrounds.

646

647 **Construction of deletion/depletion plasmids and strains.** Vectors for gene deletion by allelic
648 exchange were constructed using recommended methods for *A. tumefaciens* [78]. Briefly, 500 bp
649 fragments upstream and downstream of the target gene were amplified using primer pairs P1/P2
650 and P3/P4 respectively. Amplicons were spliced together by SOEing using primer pair P1/P4.
651 The amplicon was digested and ligated into pNTPS139. The deletion plasmids were introduced
652 into *A. tumefaciens* by mating using an *E. coli* S17 conjugation strain to create KM resistant,
653 sucrose sensitive primary exconjugants. Primary exconjugants were grown overnight in media
654 with no selection. Secondary recombinants were screened by patching for sucrose resistance and
655 KM sensitivity. Colony PCR with primers P5/P6 for the respective gene target was used to
656 confirm deletion. PCR products from P5/P6 primer sets were sequenced to further confirm
657 deletions.

For depletion strains, target genes (*ftsZ$_{AT}$, ftsA,* and *ftsW*) were amplified, digested and ligated into either pUC18-mini-Tn*7*T-GM-P$_{lac}$ or pUC18-mini-Tn*7*T-GM-P$_{lac}$. The mini-Tn*7* vectors, along with the pTNS3 helper plasmid, were introduced into C58Δ*tetRA*::a-*att*Tn*7* as described previously [32]. Transformants were selected for gentamicin resistance and insertion of the target gene into the a-*att* site was verified by colony PCR using the tet forward and Tn7R109 primer. PCR products were sequenced to confirm insertion of the correct gene. Next, the target gene was deleted from the native locus as described above in the presence of 1 mM IPTG to drive expression of the target gene from the engineered site.

Construction of plasmids for protein expression and purification. To construct pET21a FtsZ$_{AT}$, *ftsZ$_{AT}$* was amplified from C58 genomic DNA with FtsZ$_{AT}$ For NdeI and FtsZ$_{AT}$ Rev EcoRI, digested with NdeI and EcoRI, and ligated into similarly digested pET21a. To construct pTB146 FtsZ$_1$, *ftsZ$_1$* was amplified from C58 genomic DNA with FtsZ$_1$ For SapI and FtsZ$_1$ Rev BamHI, digested with SapI and BamHI, and ligated into similarly digested pTB146. Ligation products were transformed into NEB Turbo (New England Biolabs) and selected for ampicillin resistance. Insertions were verified by colony PCR and Sanger sequencing. Primers FtsZ$_{AT}$-L72W and FtsZ1-L71W were used to mutagenize pET21a FtsZ$_{AT}$ and pTB146 FtsZ$_1$, respectively, using the Quikchange Multi Lightning Mutagenesis Kit (Agilent) and following the manufacturer's protocol to generate pET21a FtsZ$_{AT}$-L72W and pTB146 FtsZ$_1$-L71W. Mutations in the targeted sites were verified by Sanger sequencing.

pET21c FtsZ$_{AT}$+CTL and pET21c FtsZ$_{AT}$ΔCTL were constructed in several steps. First, the GTPase domain of *ftsZ$_{AT}$* was amplified from C58 genomic DNA using FtsZ$_{AT}$ For NdeI and FtsZ$_{AT}$ GTPase Rev KpnI SacI, split into two aliquots, and digested with NdeI and KpnI or NdeI

and SacI. The CTL region of *ftsZ$_{AT}$* was amplified from C58 genomic DNA using FtsZ$_{AT}$ CTL For KpnI and FtsZ$_{AT}$ CTL Rev SacI and digested with KpnI and SacI. For FtsZ$_{AT}$+CTL, the GTPase domain amplicon (digested with NdeI and KpnI) was combined with the CTL amplicon (digested with KpnI and SacI) and together they were ligated into pXCFPN-1 [79] digested with NdeI and SacI. For FtsZ$_{AT}$ΔCTL, the GTPase domain amplicon (digested with NdeI and SacI) was ligated into pXCFPN-1 digested with NdeI and SacI. Each was transformed into NEB Turbo, selected for spectinomycin resistance, and confirmed by colony PCR and Sanger sequencing. Next, the CTP was added to each of the above constructs by annealing oligos FtsZ$_{AT}$ CTP + and FtsZ$_{AT}$ CTP – (engineered with overhangs compatible with SacI and NheI ligation) and ligating into the above constructs digested with SacI and NheI. Each was transformed into NEB Turbo and confirmed as above to generate pX1 FtsZ$_{AT}$+CTL and pX1 FtsZ$_{AT}$ΔCTL. Finally, FtsZ$_{AT}$+CTL and FtsZ$_{AT}$ΔCTL were subcloned into pET21c by digestion of pX1 FtsZ$_{AT}$+CTL and pX1 FtsZ$_{AT}$ΔCTL with NdeI and NheI and ligating into similarly digested pET21c. Each was transformed into NEB Turbo, selected for ampicillin resistance, and confirmed by colony PCR and Sanger sequencing.

DIC and phase contrast microscopy. Exponentially growing cells (OD_{600} = ~0.6) were spotted on 1% agarose ATGN pads as previously described [80]. Microscopy was performed with an inverted Nikon Eclipse TiE with a QImaging Rolera em-c^2 1K EMCCD camera and Nikon Elements Imaging Software. For time-lapse microscopy, images were collected every ten minutes, unless otherwise stated.

703 **Fluorescence microscopy.** Plasmid encoded $FtsZ_{AT}$-sfGFP, $FtsZ_1$-sfGFP, $FtsZ_3$-sfGFP, and
704 $LDTP_{0845}$-sfGFP fusions were expressed from the P_{van} promoter, which provides constitutive low
705 levels of expression (Figure 6- Figure Supplement 1C). Plasmid encoded FtsA-sfGFP and PopZ-
706 YFP fusions were expressed from the native promoters. Expression of plasmid encoded YFP-
707 ParB was induced by the presence of 0.1 mM cumate for 2 hours (h). Cells containing plasmids
708 with fluorescent protein fusions were grown to exponential phase before imaging on agarose
709 pads.

710 To visualize DNA, 1 ml of exponentially growing cells was treated with 1 µl of Sytox Orange
711 for 5 minutes. Cells were collected by centrifugation and washed with PBS 2 times followed by a
712 final resuspension in PBS. Cells were then imaged on agarose pads.

713 To visualize sites of active peptidoglycan synthesis 1 ml of exponentially growing cells was
714 labeled with the fluorescent D-amino acid (FDAA), HCC amino-D-alanine (HADA), as
715 previously described [49, 80].

716

717 **Cell viability and growth curve assays.** For cell viability spot assays, exponentially growing
718 cultures were diluted to OD_{600} = 0.1 and serially diluted in ATGN. 3 µl of each dilution was
719 spotted onto ATGN and incubated at 28°C for 3 days before imaging. When appropriate ATGN
720 plates contained KM 300 µg/ml, IPTG 1mM, and cumate 0.1 mM as indicated in figure legends.
721 For growth curve analysis, exponentially growing cultures were diluted to OD_{600} = .05 in 200 µl
722 of ATGN in 96-well plates. Plates were shaken for 1 minute before OD_{600} readings, which were
723 taken every 10 minutes.

724

725 **Cell morphology and constriction rate analysis.** Exponentially growing cells were imaged
726 using phase contrast microscopy as described above. Cell length, area, and constrictions were
727 detected using MicrobeJ software [81].

728 To calculate constriction rates, cells with detectable constrictions were tracked using time-lapse
729 microscopy. The width of the cell constriction was measured at an initial time-point and the
730 measurement was repeated after 10 minutes. The difference in constriction width was divided by
731 the 10-minute time interval to give a constriction rate.

732

733 **Western blot analysis.** For western blot analysis of FtsZ depletion, the *ftsZ* depletion strain was
734 grown in 40 ml ATGN with 1 mM IPTG to exponential phase. 2 ml of culture was collected
735 prior to depletion (time 0) by centrifugation at 10,000 x *g* for 3 minutes. The remaining culture
736 was collected by centrifugation at 3500 x *g* for 10 minutes, and supernatants were discarded.
737 Cells were washed in sterile water and pelleted again. To deplete FtsZ, the pellet was
738 resuspended in fresh ATGN without IPTG and grown under standard culturing conditions. 2-ml
739 samples were collected by centrifugation after 30, 45, 60, 120, and 240 minutes of depletion.
740 OD_{600} was taken for each sample prior to centrifugation so that samples could be normalized to
741 an OD_{600} equivalent to 0.68. The cell pellets were incubated with 100 µl of a master mix
742 containing 1 ml of BugBuster protein extraction reagent (Novagen) and supplemented with 1
743 EDTA-free protease inhibitor cocktail (Sigma), 10 µl of lysonase (Novagen), 2,500 U/ml DNase
744 I (Thermo Scientific), and 1 mM dithiothreitol (DTT) (Thermo Scientific) for 25 minutes with
745 shaking at room temperature to lyse the cell pellets. The whole-cell lysates were clarified by
746 centrifugation at 10,000 rpm for 15 min. A final concentration of 1 X Laemmli buffer was added
747 to the cleared cell lysates. Samples were boiled at 100°C for 5 min prior to loading on a 4-15%

748 Mini-PROTEAN TGX Precast Gel (Bio-Rad). The separated proteins were electroblotted onto
749 polyvinylidene difluoride (PVDF) membranes (Bio-Rad) and blocked overnight in 5% nonfat
750 dry milk powder solubilized in 1% TBST (Tris-buffered saline [TBS], 1% Tween 20). The
751 blocked PVDF membranes were probed with *Escherichia coli* anti-FtsZ (1:3000) monoclonal
752 antibody (gift from Joe Lutkenhaus) for 1.5 h in 5% milk-TBST, followed by incubation with
753 anti-rabbit (1:5000) HRP (Pierce 31460) secondary antibody for 1 h in 5% milk-TBST. The
754 secondary antibody was detected using the ECL Plus HRP substrate (Thermo Scientific Pierce).
755
756 For comparison of expression from P_{van}, P_{lac}, and P_{cym} promoters, strains were grown in 2 ml
757 ATGN with 200 ug/mL KM to exponential phase. P_{lac} and P_{cym} were induced with 1 mM IPTG
758 and 50 μM cumate, respectively for 4 h. Cell pellets were lysed as described above and clarified
759 whole-cell lysates were boiled with 1 X Laemmli buffer for 5 min prior to loading on 4-15%
760 Mini-PROTEAN TGX Precast Gel (Bio-Rad). The separated proteins were electroblotted onto
761 PVDF membranes (Bio-Rad), blocked as described above, and probed with anti-GFP (1:3,000)
762 monoclonal antibody (Thermo Scientific Pierce) for 1 h in 5% milk-TBST, followed by
763 incubation with a donkey anti-mouse (1:300) horseradish peroxidase-conjugated secondary
764 antibody (Thermo Scientific Pierce) for 1 h in 5% milk-TBST. The secondary antibody was
765 detected using the ECL Plus HRP substrate (Thermo Scientific Pierce).
766
767 **Protein expression and purification.** $FtsZ_{AT}$, $FtsZ_{AT}$-L72W, $FtsZ_{AT}$+CTL ($FtsZ_{AT}$ with
768 restriction sites flanking the CTL), and $FtsZ_{AT}\Delta CTL$ ($FtsZ_{AT}$ with the CTL deleted, containing
769 the same restriction sites at the GTPase-CTC junction as in $FtsZ_{AT}$+CTL) were expressed and
770 purified in untagged form. Each was produced from a pET21 expression vector (pEG1555 –

771 $FtsZ_{AT}$, pEG1556 - $FtsZ_{AT}$-L72W, pEG1444 - $FtsZ_{AT}$+CTL, pEG1445 - $FtsZ_{AT}\Delta$CTL) in
772 *Escherichia coli* Rosetta(DE3)pLysS induced at 37°C for 4 h with 0.5 mM IPTG after OD
773 reached 0.8 to 1.0 OD at 600 nm. Cells were harvested by centrifugation at 6000 x g and
774 resuspended in 30 mL FtsZ QA buffer (50 mM Tris-HCl pH 8, 50 mM KCl, 0.1 mM EDTA,
775 10% glycerol) per liter of culture. Resuspensions were snap frozen in liquid nitrogen and stored
776 at -80°C until purification. To purify, resuspensions were thawed quickly and cells were lysed by
777 incubation with 1 mg/mL lysozyme, 2.5 mM $MgCl_2$, DNAse I, 2 mM PMSF, and a cOmplete
778 mini EDTA-free protease inhibitor tablet (Roche) for 45 min to 1 h at room temperature
779 followed by sonication. Lysates were cleared by centrifugation at 15000 x g for 30 min at 4°C
780 and filtered through a 0.45 µm filter before anion exchange chromatography (HiTrap Q HP 5
781 mL, GE Life Sciences). Protein was eluted with a linear KCl gradient (FtsZ QA buffer with 50 to
782 500 mM KCl) and fractions containing FtsZ were verified by SDS-PAGE, pooled, and subjected
783 to ammonium sulfate precipitation. Precipitates (at 17-20% ammonium sulfate saturation
784 depending on the variant) were verified by SDS-PAGE, resuspended in HEK50G (50 mM
785 HEPES-KOH pH 7.2, 0.1 mM EDTA, 50 mM KCL, 10% glycerol, 1 mM β-mercaptoethanol),
786 and further purified by gel filtration (Superdex 200 10/300 GL, GE Life Sciences). Peak
787 fractions were pooled, snap frozen in liquid nitrogen, and stored at -80°C.

788

789 $FtsZ_1$ and $FtsZ_1$-L71W were produced as His_6-SUMO fusions and cleaved to yield untagged,
790 scarless proteins. Each was produced from a pTB146 expression vector (pEG1535 - $FtsZ_1$,
791 pEG1542 - $FtsZ_1$-L71W) in *E. coli* Rosetta (DE3)pLysS as described above. Cells were
792 harvested by centrifugation as above, resuspended in HK300G (50 mM HEPES-KOH pH7.2,
793 300 mM KCl, 10% glycerol) with 20 mM imidazole, snap frozen in liquid nitrogen, and stored at

-80°C until purification. To purify, resuspensions were thawed quickly and cells were lysed by incubation with 1 mg/mL lysozyme, 2.5 mM $MgCl_2$, and DNAse I for 45 min at room temperature followed by sonication. Lysate was cleared and filtered as described above. Protein was isolated by Ni^{2+} affinity chromatography (HisTrap FF 1 mL, GE Life Sciences) and eluted in HK300G with 300 mM imidazole. Fractions containing His_6-SUMO fusions were verified by SDS-PAGE, combined with Ulp1 Sumo protease at a 1:100 (protease:FtsZ) molar ratio, and cleaved by incubation at 30°C for 3.5 h. Cleaved $FtsZ_1$ or $FtsZ_1$L71W was purified away from His_6-SUMO by gel filtration (Superdex 200 10/300 GL, GE Life Sciences) in HEK50G. Peak fractions were pooled, snap frozen in liquid nitrogen, and stored at -80°C.

Polymerization kinetics assays. A Fluoromax-3 spectrofluorometer (Jobin Yvon, Inc) was used to monitor FtsZ polymerization by right-angle light scattering and tryptophan fluorescence. $FtsZ_1$ and/or $FtsZ_{AT}$ (wild-type or L71W/L72W mutants, as indicated in figures and text) was polymerized in HEK50 (50 mM HEPES-KOH pH 7.2, 50 mM KCl, 0.1 mM EDTA) with 2.5 mM $MgCl_2$. 2 mM GTP was used to induce polymerization for light scattering and 50 μM GTP was used to induce polymerization for tryptophan fluorescence (GTP is fluorescent at the wavelengths used, so low concentrations must be used). GTP was added after baseline light scatter or fluorescence was established. For light scattering, samples were excited at 350 nm and scatter was detected at 350 nm with slits set to 2 nm. For tryptophan fluorescence, samples were excited at 295 nm and emission was detected at 344 nm, with 2 nm slits.

GTPase assay. $FtsZ_1$ and/or $FtsZ_{AT}$ was polymerized in HEK50 with 2.5 mM $MgCl_2$ and 2 mM GTP. $FtsZ_{AT}$+CTL or $FtsZ_{AT}$ΔCTL was polymerized in HEK50 or HEK300 (same as HEK50 but with 300 mM KCl) as indicated, with 10 mM $MgCl_2$ and 2 mM GTP. GTP was added at time 0. Reaction was stopped at 5, 10, 15, 20, and 30 minutes with quench buffer (50 mM HEPES-KOH pH 7.2, 21.3 mM EDTA, 50 mM KCl). Inorganic phosphate in solution (liberated by GTP hydrolysis) over time was measured using SensoLyte MG Phosphate Assay Kit Colorimetric (AnaSpec, Inc, Fremont, California).

Negative stain transmission electron microscopy (TEM). $FtsZ_1$ and/or $FtsZ_{AT}$ were polymerized in HEK50 with 2.5 mM $MgCl_2$ and 2 mM GTP. 4 μM $FtsZ_{AT}$+CTL or $FtsZ_{AT}$ΔCTL were polymerized in HEK50 or HEK300 as indicated with 10 mM $MgCl_2$ and 2 mM GTP. After a 15-minute incubation at room temperature, samples were applied to carbon-coated glow-discharged grids with 0.75% uranyl formate staining as previously described [17, 82]. TEM samples were imaged using a Philips/FEI BioTwin CM120 TEM equipped with an AMT XR80 8 megapixel CCD camera (AMT Imaging, USA).

Peptidoglycan composition analysis

Six cultures of WT and *ftsZ* depletion cells were grown in 10 ml of ATGN with IPTG to exponential phase. The 10 ml cell cultures were added to 40 ml of fresh media. The 50 ml cultures were grown to exponential phase and pelleted by centrifugation at 4000 x *g* for 10 minutes. Cell pellets were washed three times with ATGN by centrifugation and resuspension to remove IPTG. After the final wash 3 cell pellets were resuspended in 50 ml ATGN and the remaining 3 pellets

were resuspended in 50 ml ATGN with 1 mM IPTG. Each culture was grown for 14 h. The optical densities of the cells were monitored to ensure the optical density of the cultures never went above OD_{600} = 0.7 to avoid changes to peptidoglycan content due to stationary phase. If necessary, fresh medium was added to dilute the cultures to maintain exponential growth. After 14 h of growth, 50 ml of the exponential cultures were collected and pelleted by centrifugation at 4000 x *g* for 20 minutes. Cell pellets were resuspended in 1mL of ATGN and 2 mL of 6% SDS and stirred with magnets while boiling for 4 h. After 4 h, samples were removed from heat but continued to stir overnight. Samples were then shipped to Dr. Felipe Cava's laboratory for purification and analysis.

Upon arrival, cells were boiled and simultaneously stirred by magnets for 2 h. After 2 h, boiling was stopped and samples were stirred overnight. Peptidoglycan was pelleted by centrifugation for 13 min at 60000 rpm (TLA100.3 Beckman rotor, Optima Max-TL ultracentrifuge; Beckman), and the pellets were washed 3 to 4 times by repeated cycles of centrifugation and resuspension in water. The pellet from the final wash was resuspended in 50 µl of 50 mM sodium phosphate buffer, pH 4.9, and digested overnight with 100 µg/ml of muramidase at 37°C. Muramidase digestion was stopped by boiling for 4 min. Coagulated protein was removed by centrifugation for 15 min at 15000 rpm in a desktop microcentrifuge. The muropeptides were mixed with 15 µl 0.5 M sodium borate and subjected to reduction of muramic acid residues into muramitol by sodium borohydride (10 mg/ml final concentration, 20 min at room temperature) treatment. Samples were adjusted to pH 3 to 4 with orthophosphoric acid and filtered (0.2-µm filters).

Muropeptides were analyzed on a Waters UPLC system equipped with an ACQUITY UPLC BEH C18 Column, 130 Å, 1.7 µm, 2.1 mm × 150 mm (Waters) and a dual wavelength absorbance

860 detector. Elution of muropeptides was detected at 204 nm. Muropeptides were separated at 45°C
861 using a linear gradient from buffer A [formic acid 0.1% (v/v)] to buffer B [formic acid 0.1% (v/v),
862 acetonitrile 20% (v/v)] in a 12 min run with a 0.250 ml/min flow. Peptidoglycan compositional
863 analysis on triplicate samples was completed on two separate occasions.
864

865 **ACKNOWLEDGEMENTS**

866 We thank members of the Brown lab for helpful discussions and critical reading of this
867 manuscript.

868

869 **FUNDING INFORMATION**

870 PB and MH were supported by the National Science Foundation, IOS1557806. This work was
871 funded in part by the National Institutes of Health through R01GM108640 (EDG) and
872 T32GM007445 (training support of PJL). FC and AA receive funding support from Laboratory
873 for Molecular Infection Medicine Sweden, Knut and Alice Wallenberg Foundation, Kempe and
874 the Swedish Research Council. AA is supported by a MIMS/VR PhD position.

875

References

1. den Blaauwen T, Andreu JM, Monasterio O. Bacterial cell division proteins as antibiotic targets. Bioorg Chem. 2014;55:27-38. Epub 2014/04/24. doi: 10.1016/j.bioorg.2014.03.007. PMID: 24755375.

2. Haeusser DP, Levin PA. The great divide: coordinating cell cycle events during bacterial growth and division. Curr Opin Microbiol. 2008;11(2):94-9. Epub 2008/04/09. doi: 10.1016/j.mib.2008.02.008. PMID: 18396093.

3. Wu LJ, Errington J. Coordination of cell division and chromosome segregation by a nucleoid occlusion protein in *Bacillus subtilis*. Cell. 2004;117(7):915-25. Epub 2004/06/24. doi: 10.1016/j.cell.2004.06.002. PMID: 15210112.

4. Bi EF, Lutkenhaus J. FtsZ ring structure associated with division in *Escherichia coli*. Nature. 1991;354(6349):161-4. Epub 1991/11/14. doi: 10.1038/354161a0. PMID: 1944597.

5. de Boer P, Crossley R, Rothfield L. The essential bacterial cell-division protein FtsZ is a GTPase. Nature. 1992;359(6392):254-6. Epub 1992/09/17. doi: 10.1038/359254a0. PMID: 1528268.

6. Li Z, Trimble MJ, Brun YV, Jensen GJ. The structure of FtsZ filaments in vivo suggests a force-generating role in cell division. Embo j. 2007;26(22):4694-708. Epub 2007/10/20. doi: 10.1038/sj.emboj.7601895. PMID: 17948052.

7. Fu G, Huang T, Buss J, Coltharp C, Hensel Z, Xiao J. In vivo structure of the *E. coli* FtsZ-ring revealed by photoactivated localization microscopy (PALM). PLoS One. 2010;5(9):e12682. Epub 2010/09/22. doi: 10.1371/journal.pone.0012680. PMID: 20856929.

8. Holden SJ, Pengo T, Meibom KL, Fernandez Fernandez C, Collier J, Manley S. High throughput 3D super-resolution microscopy reveals *Caulobacter crescentus* in vivo Z-ring

899 organization. Proc Natl Acad Sci U S A. 2014;111(12):4566-71. Epub 2014/03/13. doi:
900 10.1073/pnas.1313368111. PMID: 24616530.
901 9. Bisson-Filho AW, Hsu YP, Squyres GR, Kuru E, Wu F, Jukes C, et al. Treadmilling by
902 FtsZ filaments drives peptidoglycan synthesis and bacterial cell division. Science.
903 2017;355(6326):739-43. Epub 2017/02/18. doi: 10.1126/science.aak9973. PMID: 28209898.
904 10. Yang X, Lyu Z, Miguel A, McQuillen R, Huang KC, Xiao J. GTPase activity-coupled
905 treadmilling of the bacterial tubulin FtsZ organizes septal cell wall synthesis. Science.
906 2017;355(6326):744-7. Epub 2017/02/18. doi: 10.1126/science.aak9995. PMID: 28209899.
907 11. Du S, Lutkenhaus J. Assembly and activation of the *Escherichia coli* divisome. Mol
908 Microbiol. 2017;105(2):177-87. doi: doi:10.1111/mmi.13696.
909 12. Meier EL, Goley ED. Form and function of the bacterial cytokinetic ring. Curr Opin Cell
910 Biol. 2014;26:19-27. Epub 2014/02/18. doi: 10.1016/j.ceb.2013.08.006. PMID: 24529242.
911 13. Goley ED, Yeh YC, Hong SH, Fero MJ, Abeliuk E, McAdams HH, et al. Assembly of
912 the *Caulobacter* cell division machine. Mol Microbiol. 2011;80(6):1680-98. Epub 2011/05/06.
913 doi: 10.1111/j.1365-2958.2011.07677.x. PMID: 21542856.
914 14. Erickson HP, Anderson DE, Osawa M. FtsZ in bacterial cytokinesis: cytoskeleton and
915 force generator all in one. Microbiol Mol Biol Rev. 2010;74(4):504-28. Epub 2010/12/02. doi:
916 10.1128/mmbr.00021-10. PMID: 21119015.
917 15. Varma A, Young KD. FtsZ collaborates with penicillin binding proteins to generate
918 bacterial cell shape in *Escherichia coli*. J Bacteriol. 2004;186(20):6768-74. Epub 2004/10/07.
919 doi: 10.1128/jb.186.20.6768-6774.2004. PMID: 15466028.
920 16. Aaron M, Charbon G, Lam H, Schwarz H, Vollmer W, Jacobs-Wagner C. The tubulin
921 homologue FtsZ contributes to cell elongation by guiding cell wall precursor synthesis in

Caulobacter crescentus. Mol Microbiol. 2007;64(4):938-52. Epub 2007/05/16. doi: 10.1111/j.1365-2958.2007.05720.x. PMID: 17501919.

17. Sundararajan K, Miguel A, Desmarais SM, Meier EL, Huang KC, Goley ED. The bacterial tubulin FtsZ requires its intrinsically disordered linker to direct robust cell wall construction. Nat Commun. 2015;6:7281. doi: 10.1038/ncomms8281. PMID: 26099469.

18. Aarsman ME, Piette A, Fraipont C, Vinkenvleugel TM, Nguyen-Disteche M, den Blaauwen T. Maturation of the *Escherichia coli* divisome occurs in two steps. Mol Microbiol. 2005;55(6):1631-45. Epub 2005/03/09. doi: 10.1111/j.1365-2958.2005.04502.x. PMID: 15752189.

19. Gray AN, Egan AJ, Van't Veer IL, Verheul J, Colavin A, Koumoutsi A, et al. Coordination of peptidoglycan synthesis and outer membrane constriction during *Escherichia coli* cell division. Elife. 2015;4. Epub 2015/05/08. doi: 10.7554/eLife.07118. PMID: 25951518.

20. Pini F, De Nisco NJ, Ferri L, Penterman J, Fioravanti A, Brilli M, et al. Cell cycle control by the master regulator CtrA in *Sinorhizobium meliloti*. PLOS Genetics. 2015;11(5):e1005232. doi: 10.1371/journal.pgen.1005232.

21. Howell M, Brown PJB. Building the bacterial cell wall at the pole. Current Opinion in Microbiology. 2016;34:53-9. doi: 10.1016/j.mib.2016.07.021.

22. Pini F, Frage B, Ferri L, De Nisco NJ, Mohapatra SS, Taddei L, et al. The DivJ, CbrA and PleC system controls DivK phosphorylation and symbiosis in *Sinorhizobium meliloti*. Mol Microbiol. 2013;90(1):54-71. Epub 2013/08/06. doi: 10.1111/mmi.12347. PMID: 23909720.

23. Bellefontaine AF, Pierreux CE, Mertens P, Vandenhaute J, Letesson JJ, De Bolle X. Plasticity of a transcriptional regulation network among alpha-proteobacteria is supported by the

identification of CtrA targets in *Brucella abortus*. Mol Microbiol. 2002;43(4):945-60. Epub 2002/04/04. PMID: 11929544.

24. Cheng J, Sibley CD, Zaheer R, Finan TM. A *Sinorhizobium meliloti* minE mutant has an altered morphology and exhibits defects in legume symbiosis. Microbiology. 2007;153(Pt 2):375-87. Epub 2007/01/30. doi: 10.1099/mic.0.2006/001362-0. PMID: 17259609.

25. Latch JN, Margolin W. Generation of buds, swellings, and branches instead of filaments after blocking the cell cycle of *Rhizobium meliloti*. J Bacteriol. 1997;179(7):2373-81. Epub 1997/04/01. PMID: 9079925.

26. Fujiwara T, Fukui S. Effect OF D-alanine and mitomycin-c on cell morphology of *Agrobacterium tumefaciens*. Gen App Microbiol. 1974;20(6):345-9. doi: 10.2323/jgam.20.345.

27. Zupan JR, Cameron TA, Anderson-Furgeson J, Zambryski PC. Dynamic FtsA and FtsZ localization and outer membrane alterations during polar growth and cell division in *Agrobacterium tumefaciens*. Proc Natl Acad Sci U S A. 2013;110(22):9060-5. doi: 10.1073/pnas.1307241110. PMID: 23674672.

28. Figueroa-Cuilan WM, Brown PJB. Cell wall biogenesis during elongation and division in the plant pathogen *Agrobacterium tumefaciens*. Curr Top Microbiol Immunol. 2018. Epub 2018/05/29. doi: 10.1007/82_2018_92. PMID: 29808336.

29. Brown PJB, de Pedro MA, Kysela DT, Van der Henst C, Kim J, De Bolle X, et al. Polar growth in the Alphaproteobacterial order Rhizobiales. Proc Natl Acad Sci U S A. 2012;109(5):1697-701. doi: 10.1073/pnas.1114476109.

30. Cameron TA, Anderson-Furgeson J, Zupan JR, Zik JJ, Zambryski PC. Peptidoglycan synthesis machinery in *Agrobacterium tumefaciens* during unipolar growth and cell division. mBio. 2014;5(3). doi: 10.1128/mBio.01219-14. PMID: 24865559.

967 31. Goley ED, Dye NA, Werner JN, Gitai Z, Shapiro L. Imaging-based identification of a
968 critical regulator of FtsZ protofilament curvature in *Caulobacter*. Mol Cell. 2010;39(6):975-87.
969 Epub 2010/09/25. doi: 10.1016/j.molcel.2010.08.027. PMID: 20864042.
970 32. Figueroa-Cuilan W, Daniel JJ, Howell M, Sulaiman A, Brown PJ. Mini-Tn*7* Insertion in
971 an artificial *att*Tn*7* site enables depletion of the essential master regulator CtrA in the
972 phytopathogen *Agrobacterium tumefaciens*. Appl Environ Microbiol. 2016;82(16):5015-25.
973 Epub 2016/06/12. doi: 10.1128/aem.01392-16. PMID: 27287320.
974 33. Ortiz C, Natale P, Cueto L, Vicente M. The keepers of the ring: regulators of FtsZ
975 assembly. FEMS Microbiol Rev. 2016;40(1):57-67. Epub 2015/09/18. doi:
976 10.1093/femsre/fuv040. PMID: 26377318.
977 34. Wood DW, Setubal JC, Kaul R, Monks DE, Kitajima JP, Okura VK, et al. The genome
978 of the natural genetic engineer *Agrobacterium tumefaciens* C58. Science. 2001;294(5550):2317-
979 23. Epub 2001/12/18. doi: 10.1126/science.1066804. PMID: 11743193.
980 35. Goodner B, Hinkle G, Gattung S, Miller N, Blanchard M, Qurollo B, et al. Genome
981 sequence of the plant pathogen and biotechnology agent *Agrobacterium tumefaciens* C58.
982 Science. 2001;294(5550):2323-8. Epub 2001/12/18. doi: 10.1126/science.1066803. PMID:
983 11743194.
984 36. Curtis PD, Brun YV. Identification of essential alphaproteobacterial genes reveals
985 operational variability in conserved developmental and cell cycle systems. Mol Microbiol.
986 2014;93(4):713-35. doi: 10.1111/mmi.12686.
987 37. Vaughan S, Wickstead B, Gull K, Addinall SG. Molecular evolution of FtsZ protein
988 sequences encoded within the genomes of archaea, bacteria, and eukaryota. J Mol Evol.
989 2004;58(1):19-29. Epub 2004/01/27. doi: 10.1007/s00239-003-2523-5. PMID: 14743312.

990 38. Margolin W, Long SR. *Rhizobium meliloti* contains a novel second homolog of the cell
991 division gene ftsZ. J Bacteriol. 1994;176(7):2033-43. Epub 1994/04/01. PMID: 8144471.
992 39. Muller FD, Raschdorf O, Nudelman H, Messerer M, Katzmann E, Plitzko JM, et al. The
993 FtsZ-like protein FtsZm of *Magnetospirillum gryphiswaldense* likely interacts with its generic
994 homolog and is required for biomineralization under nitrate deprivation. J Bacteriol.
995 2014;196(3):650-9. Epub 2013/11/26. doi: 10.1128/jb.00804-13. PMID: 24272781.
996 40. Chen Y, Bjornson K, Redick SD, Erickson HP. A rapid fluorescence assay for FtsZ
997 assembly indicates cooperative assembly with a dimer nucleus. Biophys J. 2005;88(1):505-14.
998 Epub 2004/10/12. doi: 10.1529/biophysj.104.044149. PMID: 15475583.
999 41. Olson BJ, Wang Q, Osteryoung KW. GTP-dependent heteropolymer formation and
1000 bundling of chloroplast FtsZ1 and FtsZ2. J Biol Chem. 2010;285(27):20634-43. Epub
1001 2010/04/28. doi: 10.1074/jbc.M110.122614. PMID: 20421292.
1002 42. El-Kafafi el S, Mukherjee S, El-Shami M, Putaux JL, Block MA, Pignot-Paintrand I, et
1003 al. The plastid division proteins, FtsZ1 and FtsZ2, differ in their biochemical properties and sub-
1004 plastidial localization. Biochem J. 2005;387(Pt 3):669-76. Epub 2004/12/17. doi:
1005 10.1042/bj20041281. PMID: 15601251.
1006 43. TerBush AD, MacCready JS, Chen C, Ducat DC, Osteryoung KW. Conserved dynamics
1007 of chloroplast cytoskeletal FtsZ proteins across photosynthetic lineages. Plant Physiol.
1008 2018;176(1):295-306. Epub 2017/08/18. doi: 10.1104/pp.17.00558. PMID: 28814573.
1009 44. Richards DM, Hempel AM, Flardh K, Buttner MJ, Howard M. Mechanistic basis of
1010 branch-site selection in filamentous bacteria. PLoS Comput Biol. 2012;8(3):e1002423. Epub
1011 2012/03/17. doi: 10.1371/journal.pcbi.1002423. PMID: 22423220.

1012 45. Howell M, Aliashkevich A, Salisbury AK, Cava F, Bowman GR, Brown PJB. Absence
1013 of the polar organizing protein PopZ results in reduced and asymmetric cell division in
1014 *Agrobacterium tumefaciens*. J Bacteriol. 2017;199(17). Epub 2017/06/21. doi: 10.1128/jb.00101-
1015 17. PMID: 28630123.
1016 46. Ehrle HM, Guidry JT, Iacovetto R, Salisbury AK, Sandidge DJ, Bowman GR. Polar
1017 organizing protein PopZ is required for chromosome segregation in *Agrobacterium tumefaciens*.
1018 J Bacteriol. 2017;199(17). Epub 2017/06/21. doi: 10.1128/jb.00111-17. PMID: 28630129.
1019 47. Grangeon R, Zupan JR, Anderson-Furgeson J, Zambryski PC. PopZ identifies the new
1020 pole, and PodJ identifies the old pole during polar growth in *Agrobacterium tumefaciens*. Proc
1021 Natl Acad Sci U S A. 2015;112(37):11666-71. Epub 2015/09/02. doi: 10.1073/pnas.1515544112.
1022 PMID: 26324921.
1023 48. Thanbichler M. Synchronization of chromosome dynamics and cell division in bacteria.
1024 Cold Spring Harb Perspect Biol. 2010;2(1):a000331. Epub 2010/02/26. doi:
1025 10.1101/cshperspect.a000331. PMID: 20182599.
1026 49. Kuru E, Velocity Hughes H, Brown PJ, Hall E, Tekkam S, Cava F, et al. *In situ* probing
1027 of newly synthesized peptidoglycan in live bacteria with fluorescent D-amino acids. Angew
1028 Chem Int Ed Engl. 2012;51(50):12519-23. doi: 10.1002/anie.201206749. PMID: 23055266.
1029 50. Alvarez L, Hernandez SB, de Pedro MA, Cava F. Ultra-sensitive, high-resolution liquid
1030 chromatography methods for the high-throughput quantitative analysis of bacterial cell wall
1031 chemistry and structure. Methods Mol Biol. 2016;1440:11-27. Epub 2016/06/18. doi:
1032 10.1007/978-1-4939-3676-2_2. PMID: 27311661.
1033 51. Szwedziak P, Wang Q, Freund SM, Lowe J. FtsA forms actin-like protofilaments. Embo
1034 j. 2012;31(10):2249-60. Epub 2012/04/05. doi: 10.1038/emboj.2012.76. PMID: 22473211.

1035 52. Ma X, Margolin W. Genetic and functional analyses of the conserved C-terminal core
1036 domain of *Escherichia coli* FtsZ. J Bacteriol. 1999;181(24):7531-44. Epub 1999/12/22. PMID:
1037 10601211.
1038 53. Sundararajan K, Goley ED. The intrinsically disordered C-terminal linker of FtsZ
1039 regulates protofilament dynamics and superstructure in vitro. J Biol Chem. 2017;292(50):20509-
1040 27. Epub 2017/11/02. doi: 10.1074/jbc.M117.809939. PMID: 29089389.
1041 54. Buske PJ, Levin PA. A flexible C-terminal linker is required for proper FtsZ assembly in
1042 vitro and cytokinetic ring formation in vivo. Mol Microbiol. 2013;89(2):249-63. Epub
1043 2013/05/23. doi: 10.1111/mmi.12272. PMID: 23692518.
1044 55. Gardner KA, Moore DA, Erickson HP. The C-terminal linker of *Escherichia coli* FtsZ
1045 functions as an intrinsically disordered peptide. Mol Microbiol. 2013;89(2):264-75. Epub
1046 2013/05/30. doi: 10.1111/mmi.12279. PMID: 23714328.
1047 56. Khan SR, Gaines J, Roop RM, 2nd, Farrand SK. Broad-host-range expression vectors
1048 with tightly regulated promoters and their use to examine the influence of TraR and TraM
1049 expression on Ti plasmid quorum sensing. Appl Environ Microbiol. 2008;74(16):5053-62. Epub
1050 2008/07/09. doi: 10.1128/aem.01098-08. PMID: 18606801.
1051 57. Kaczmarczyk A, Vorholt JA, Francez-Charlot A. Cumate-inducible gene expression
1052 system for sphingomonads and other alphaproteobacteria. Appl Environ Microbiol.
1053 2013;79(21):6795-802. Epub 2013/09/03. doi: 10.1128/aem.02296-13. PMID: 23995928.
1054 58. Eaton RW. p-Cumate catabolic pathway in *Pseudomonas putida* Fl: cloning and
1055 characterization of DNA carrying the cmt operon. J Bacteriol. 1996;178(5):1351-62. Epub
1056 1996/03/01. PMID: 8631713.

1057 59. Wang X, Huang J, Mukherjee A, Cao C, Lutkenhaus J. Analysis of the interaction of
1058 FtsZ with itself, GTP, and FtsA. J Bacteriol. 1997;179(17):5551-9. Epub 1997/09/01. PMID:
1059 9287012.
1060 60. Pichoff S, Lutkenhaus J. Identification of a region of FtsA required for interaction with
1061 FtsZ. Mol Microbiol. 2007;64(4):1129-38. Epub 2007/05/16. doi: 10.1111/j.1365-
1062 2958.2007.05735.x. PMID: 17501933.
1063 61. Moll A, Thanbichler M. FtsN-like proteins are conserved components of the cell division
1064 machinery in proteobacteria. Mol Microbiol. 2009;72(4):1037-53. Epub 2009/04/30. doi:
1065 10.1111/j.1365-2958.2009.06706.x. PMID: 19400794.
1066 62. Cameron TA, Zupan JR, Zambryski PC. The essential features and modes of bacterial
1067 polar growth. Trends in Microbiology. 2015;23(6):347-53. doi: 10.1016/j.tim.2015.01.003.
1068 63. Meier EL, Razavi S, Inoue T, Goley ED. A novel membrane anchor for FtsZ is linked to
1069 cell wall hydrolysis in *Caulobacter crescentus*. Mol Microbiol. 2016;101(2):265-80. Epub
1070 2016/03/31. doi: 10.1111/mmi.13388. PMID: 27028265.
1071 64. Fraipont C, Alexeeva S, Wolf B, van der Ploeg R, Schloesser M, den Blaauwen T, et al.
1072 The integral membrane FtsW protein and peptidoglycan synthase PBP3 form a subcomplex in
1073 *Escherichia coli*. Microbiology. 2011;157(Pt 1):251-9. Epub 2010/09/18. doi:
1074 10.1099/mic.0.040071-0. PMID: 20847002.
1075 65. Grangeon R, Zupan J, Jeon Y, Zambryski PC. Loss of PopZ At activity in *Agrobacterium*
1076 *tumefaciens* by Deletion or Depletion Leads to Multiple Growth Poles, Minicells, and Growth
1077 Defects. MBio. 2017;8(6). Epub 2017/11/16. doi: 10.1128/mBio.01881-17. PMID: 29138309.

66. Rowlett VW, Margolin W. The Min system and other nucleoid-independent regulators of Z ring positioning. Front Microbiol. 2015;6:478. Epub 2015/06/02. doi: 10.3389/fmicb.2015.00478. PMID: 26029202.

67. Monahan LG, Hajduk IV, Blaber SP, Charles IG, Harry EJ. Coordinating bacterial cell division with nutrient availability: a role for glycolysis. MBio. 2014;5(3):e00935-14. Epub 2014/05/16. doi: 10.1128/mBio.00935-14. PMID: 24825009.

68. Flores SA, Howell M, Daniel JJ, Piccolo R, Brown PJB. Absence of the Min system does not cause major cell division defects in *Agrobacterium tumefaciens*. Front Microbiol. 2018;9:681. Epub 2018/04/25. doi: 10.3389/fmicb.2018.00681. PMID: 29686659.

69. Mosyak L, Zhang Y, Glasfeld E, Haney S, Stahl M, Seehra J, et al. The bacterial cell-division protein ZipA and its interaction with an FtsZ fragment revealed by X-ray crystallography. Embo j. 2000;19(13):3179-91. Epub 2000/07/06. doi: 10.1093/emboj/19.13.3179. PMID: 10880432.

70. Haney SA, Glasfeld E, Hale C, Keeney D, He Z, de Boer P. Genetic analysis of the *Escherichia coli* FtsZ.ZipA interaction in the yeast two-hybrid system. Characterization of FtsZ residues essential for the interactions with ZipA and with FtsA. J Biol Chem. 2001;276(15):11980-7. Epub 2001/03/30. doi: 10.1074/jbc.M009810200. PMID: 11278571.

71. Cho H, Wivagg CN, Kapoor M, Barry Z, Rohs PD, Suh H, et al. Bacterial cell wall biogenesis is mediated by SEDS and PBP polymerase families functioning semi-autonomously. Nat Microbiol. 2016:16172. Epub 2016/09/20. doi: 10.1038/nmicrobiol.2016.172. PMID: 27643381.

1099 72. Meeske AJ, Riley EP, Robins WP, Uehara T, Mekalanos JJ, Kahne D, et al. SEDS
1100 proteins are a widespread family of bacterial cell wall polymerases. Nature.
1101 2016;537(7622):634-8. Epub 2016/08/16. doi: 10.1038/nature19331. PMID: 27525505.
1102 73. Emami K, Guyet A, Kawai Y, Devi J, Wu LJ, Allenby N, et al. RodA as the missing
1103 glycosyltransferase in *Bacillus subtilis* and antibiotic discovery for the peptidoglycan polymerase
1104 pathway. Nat Microbiol. 2017;2:16253. Epub 2017/01/14. doi: 10.1038/nmicrobiol.2016.253.
1105 PMID: 28085152.
1106 74. Botta GA, Park JT. Evidence for involvement of penicillin-binding protein 3 in murein
1107 synthesis during septation but not during cell elongation. J Bacteriol. 1981;145(1):333-40. Epub
1108 1981/01/01. PMID: 6450748.
1109 75. Morton ER, Fuqua C. Laboratory maintenance of *Agrobacterium*. Curr Protoc Microbiol.
1110 2012;Chapter 1:Unit3D 1. doi: 10.1002/9780471729259.mc03d01s24. PMID: 22307549.
1111 76. Choi YJ, Morel L, Le Francois T, Bourque D, Bourget L, Groleau D, et al. Novel,
1112 versatile, and tightly regulated expression system for *Escherichia coli* strains. Appl Environ
1113 Microbiol. 2010;76(15):5058-66. Epub 2010/06/22. doi: 10.1128/aem.00413-10. PMID:
1114 20562288.
1115 77. Denkovskiene E, Paskevicius S, Werner S, Gleba Y, Razanskiene A. Inducible
1116 expression of *Agrobacterium* Virulence gene VirE2 for stringent regulation of T-DNA transfer in
1117 plant transient expression systems. Mol Plant Microbe Interact. 2015;28(11):1247-55. Epub
1118 2015/08/22. doi: 10.1094/mpmi-05-15-0102-r. PMID: 26292850.
1119 78. Morton ER, Fuqua C. Unit 3D.2 genetic manipulation of *Agrobacterium*. Curr Protoc
1120 Microbiol. 2012;Chapter:Unit-3D.2. doi: 10.1002/9780471729259.mc03d02s25. PMID:
1121 22549163.

79. Thanbichler M, Iniesta AA, Shapiro L. A comprehensive set of plasmids for vanillate- and xylose-inducible gene expression in *Caulobacter crescentus*. Nucleic Acids Res. 2007;35(20):e137. Epub 2007/10/26. doi: 10.1093/nar/gkm818. PMID: 17959646.

80. Howell M, J. Daniel J, J.B. Brown P. Live cell fluorescence microscopy to observe essential processes during microbial cell growth.: J Vis Exp; 2017.

81. Ducret A, Quardokus EM, Brun YV. MicrobeJ, a tool for high throughput bacterial cell detection and quantitative analysis. Nat Microbiol. 2016;1(7):16077. Epub 2016/08/31. doi: 10.1038/nmicrobiol.2016.77. PMID: 27572972.

82. Lariviere PJ, Szwedziak P, Mahone CR, Lowe J, Goley ED. FzlA, an essential regulator of FtsZ filament curvature, controls constriction rate during *Caulobacter* division. Mol Microbiol. 2018;107(2):180-97. Epub 2017/11/10. doi: 10.1111/mmi.13876. PMID: 29119622.

Figure Legends

Figure 1. Characterization of FtsZ homologs in *A. tumefaciens*. A) Domain schematic of FtsZ homologs in *A. tumefaciens*. Note that domains are not drawn to scale. B) Representative image of localization patterns for each homolog. $FtsZ_{AT}$-sfGFP and $FtsZ_1$-sfGFP show mid-cell ring formation while $FtsZ_3$-sfGFP fails to localize. C) Cell viability is shown by spotting serial dilutions. Δ*ftsZ*$_1$, Δ*ftsZ*$_3$, and +*ftsZ*$_{AT}$ have similar viability to WT, while -*ftsZ*$_{AT}$ displays a drastic decrease in viability. D) Cell morphology and microcolony formation of Δ*ftsZ*$_1$ and Δ*ftsZ*$_3$ are similar to WT, while -*ftsZ*$_{AT}$ results in long branched cells that fail to divide. All scale bars are set to 2 μm.

Figure 1- Figure Supplement 1. Cell growth and morphology of *ftsZ* mutants. A.) Western blot analysis showing the depletion of FtZ_{AT} after the removal of inducer. B) Cell lengths of WT, Δ*ftsZ*$_1$, Δ*ftsZ*$_3$, and induced *ftsZ*$_{AT}$. are indistinguishable. C) Cell area in WT and induced *ftsZ*$_{AT}$ are the same while cells depleted of $FtsZ_{AT}$ for 8 and 14 hours accumulate cell area.

Figure 2. Deletion of multiple *ftsZ* homologs does not yield an additive effect. A) Cell viability (top) and morphology (bottom) of the double mutant Δ*ftsZ*$_1$Δ*ftsZ*$_3$ is indistinguishable from WT. B) Cell viability (top) and morphology (bottom) of Δ*ftsZ*$_1$, Δ*ftsZ*$_3$, or Δ*ftsZ*$_1$Δ*ftsZ*$_3$ during $FtsZ_{AT}$ depletion are indistinguishable from $FtsZ_{AT}$ depletion alone. All scale bars are set to 2 μm. Black bar denotes *ftsZ*$_{AT}$ depletion strain background.

Figure 3. $FtsZ_1$ requires $FtsZ_{AT}$ to polymerize *in vitro* and to localize in cells. A) $FtsZ_1$-sfGFP forms midcell rings which constrict in WT and when *ftsZ*$_{AT}$ is induced. $FtsZ_1$-sfGFP fails to constrict early rings and disassembles during $FtsZ_{AT}$ depletion. Scale bar is set to 2 μm. B)

Light scattering over time for purified proteins at the indicated concentrations. $FtsZ_{AT}$ polymerizes at concentrations above 2 μM, but $FtsZ_1$ does not polymerize. GTP (2 mM) was added where indicated by the arrow to induce polymerization. Experiments were performed in triplicate and mean curves are shown. C) Negative stain TEM of the indicated proteins. Co-polymers of $FtsZ_{AT}$ and $FtsZ_1$ are indistinguishable from $FtsZ_{AT}$ polymers. Scale bar is set to 100 nm. D) Inorganic phosphate concentration in solution over time in the presence of the indicated proteins and protein concentrations. Co-polymers of $FtsZ_{AT}$ and $FtsZ_1$ consume GTP at the same rate as $FtsZ_{AT}$ homopolymers at equivalent total FtsZ concentration. Reactions were performed in triplicate and mean ± standard error is plotted. E) Tryptophan fluorescence over time for the indicated proteins. $FtsZ_1$-L71W (red) shows no polymerization (Trp fluorescence) on its own, but can co-polymerize with added $FtsZ_{AT}$ (purple). GTP (50 μM) was added where indicated by the arrow to induce polymerization. Experiments were performed in triplicate and representative curves are shown.

Figure 4. Characterization of genomic content during $FtsZ_{AT}$ depletion. A) Timelapse microscopy in minutes demonstrates proper cell division and microcolony formation in +*ftsZ*$_{AT}$ induced with IPTG (top panel). Timelapse during depletion of $FtsZ_{AT}$ demonstrates branches forming from tip splitting events (bottom panel). B) Timelapse microscopy shows that PopZ-YFP maintains polar localization during elongation and dissociates moving to the mid-cell at division in WT and when *ftsZ*$_{AT}$ is induced. PopZ-YFP becomes trapped at the growth poles during $FtsZ_{AT}$ depletion. C) Sytox Orange labeled DNA is diffuse throughout young cells and separated nucleoids are seen in late divisional cells in WT and when $FtsZ_{AT}$ is induced. These DNA free regions are marked with an asterisk. Nucleoids fail to form, as diffuse DNA labeling is observed during $FtsZ_{AT}$ depletion at both 8 h and 14 h depletion timepoints. D) Timelapse

microscopy demonstrates YFP-ParB1 form a single focus at the old pole in WT and when *ftsZ$_{AT}$* is induced. A second focus then translocates the cell length to the growth pole. Timelape microscopy during FtsZ$_{AT}$ depletion reveals a third focus which translocates the cell towards an ectopic pole. E) Quantitation of YFP-ParB1 foci plotted against cell area. Number of foci increase as cell area increases. All scale bars are set to 2 μm.

Movie 1. Growth and morphological changes during FtsZ$_{AT}$ depletion. Cells were washed to remove inducer and grown in liquid ATGN for 4 hours before spotting on a ATGN pad. Images were acquired every ten minutes and movie is played at 10 frames per second for a total of 145 frames.

Figure 5. Characterization of polar peptidoglycan synthesis during FtsZ$_{AT}$ depletion. A) FDAA labels active peptidoglycan synthesis at a single growing pole and septum in WT and cells depleted of FtsZ$_{AT}$ for 0 h. As FtsZ$_{AT}$ is depleted for 8 and 14 h, multiple growth poles are labeled, and septum labeling is lost. B) Quantitation of the major muropeptide peaks in *ftsZ$_{AT}$* depletion strain induced and depleted. C) Abundance of total monomers, dimers, and trimers in the muropeptide profile in *ftsZ$_{AT}$* depletion strain. D) Abundance of total LD and DD crosslinkage in *ftsZ$_{AT}$* depletion strain induced. For B,C,and D, data shown are the average abundance of each muropeptide and are taken from analysis of three independent biological samples of *ftsZ$_{AT}$* depletion strain induced (black bars) and depleted for 14 h (gray bars). Statistical was calculated by t-tests and is indicated with an asterisk (P-value <0.05 (*), <0.005 (**), <0.001 (***)). E) Timelapse microscopy of LDTP$_{0845}$-sfGFP in WT and when *ftsZ$_{AT}$* is induced yields growth pole localization during elongation and mid-cell localization during septum formation. In cells depleted of FtsZ$_{AT}$, localization is trapped at the growing poles. All scale bars are set to 2 μm.

Figure 5- Figure Supplement 1. Peptidoglycan analysis of control strains. A) UPLC spectra of muropeptides derived from WT cells. Major muropeptides are labeled. M= monomers, D= dimers, T= trimers. Numbers indicate the length of the muropeptide stems and the position of crosslink in dimers and trimers. B) Quantitation of the major muropeptide peaks in WT with IPTG (black), WT without IPTG (black with gray outline), and *ftsZ*$_{AT}$ depletion strain induced with IPTG (Gray). Data shown is the average abundance of each muropeptide and is taken from analysis of three independent biological samples. Statistical significance is indicated with an asterisk.

Figure 6. Functional analysis of FtsZ$_{AT}$ΔCTL and FtsZ$_{AT}$ΔCTP. A) Cell viability is measured by spotting serial dilutions of *ftsZ*$_{AT}$ variants in the *ftsZ*$_{AT}$ depletion background. When chromosomal *ftsZ*$_{AT}$ is induced by IPTG and plasmid driven *ftsZ*$_{AT}$ variants are uninduced, all strains have similar viability (top left). When both chromosomal *ftsZ*$_{AT}$ is uninduced and plasmid driven *ftsZ*$_{AT}$ variants are uninduced, all strains exhibit an equal decrease in viability (top right). When chromosomal *ftsZ*$_{AT}$ is uninduced and plasmid driven *ftsZ*$_{AT}$ variants are induced by cumate, FtsZ$_{AT}$ expression rescues viability, FtsZ$_{AT}$ΔCTP partially rescues, and FtsZ$_{AT}$ΔCTL fails to rescue viability (bottom left). When both chromosomal *ftsZ*$_{AT}$ is induced with IPTG and plasmid driven *ftsZ*$_{AT}$ variants are induced by cumate, FtsZ$_{AT}$ΔCTL expression reduces viability while other variants have no impact (bottom right). B) Representative images displaying morphology and FDAA labeling while chromosomal *ftsZ*$_{AT}$ is uninduced and plasmid driven *ftsZ*$_{AT}$ variants are induced for 6 and 14 h. C) Timelapse microscopy while chromosomal *ftsZAT* is uninduced and plasmid driven FtsZ$_{AT}$ΔCTP is expressed reveal that polar growth fails to terminate and undergoes tip splitting, although septum formation and cell division also take place (top panel). Timelapse microscopy while chromosomal *ftsZ*$_{AT}$ is uninduced and plasmid driven

1227 $FtsZ_{AT}$ΔCTL is expressed shows termination of polar growth and new pole formation near mid-
1228 cell (bottom panel).

1229 **Figure 6- Figure Supplement 1. Validation of a cumate inducible vector in *A. tumefaciens.***
1230 A) Sequence schematic of the cumate operon modified for use is pSRKKM-*sfGFP*. Regions are
1231 color coded to match sequence found in Table S2. B) Representative image of WT cells
1232 harboring pSRKKM-Pcym-sfGFP uninduced (left) and induced (right). C) Western blot analysis
1233 comparing expression levels of sfGFP expressed from pRV, pSRKKM-Plac, and pSRKKM-
1234 Pcym. D) Growth curve analysis of WT cells harboring psRKKM-Pcym-empty induced with
1235 different levels of cumate (left). pSRKKM-Pcym-$ftsZ_{AT}$ rescues chromosomal $FtsZ_{AT}$ depletion
1236 with 0.01mM cumate (right).

1237 **Figure 7. $FtsZ_{AT}$ requires the CTL for robust PG biosynthesis and proper polymerization.**
1238 A.) Quantitation of the major muropeptide peaks in $ftsZ_{AT}$ depletion strain expressing an empty
1239 plasmid, full length $FtsZ_{AT}$, or $FtsZ_{AT}$ΔCTL. B) Abundance of total monomers, dimers, and
1240 trimers in the muropeptide profile. C) Abundance of total LD and DD crosslinkage. For A, B,
1241 and C, data shown are the average abundance of each muropeptide and are taken from analysis
1242 of three independent biological samples. Statistical significance is indicated with an asterisk. D.)
1243 Negative stain TEM of the 4 μM of the indicated protein in the presence of 50 or 300 mM KCl.
1244 $FtsZ_{AT}$ΔCTL shows increased propensity to bundle at high salt. Scale bar is set at 100 nm. E.)
1245 Phosphate in solution over time in the presence of indicated proteins in solution with 50 or 300
1246 mM KCl. The rate of GTP hydrolysis by $FtsZ_{AT}$ΔCTL is reduced under high salt conditions that
1247 promote bundling.

1248 **Figure 8. FtsA is not required for termination of polar growth.** A) FtsA-sfGFP persists at
1249 growth poles and forms mid-cell rings which constrict in WT (top panel). FtsA-sfGFP becomes

trapped at the growth poles and foci split as the growth poles split during $FtsZ_{AT}$ depletion (bottom panel). B) Timelapse microscopy shows cells expressing FtsA grow and divide normally forming microcolonies (top panel). Cells depleted of FtsA terminate polar growth and form new growth poles near the mid-cell (bottom panel). C) FDAAs label a single growth pole when FtsA is present (top) and label multiple poles emerging from the mid-cell when FtsA is absent (bottom). D) Timelapse microscopy during FtsA depletion shows PopZ-YFP localizes to the growth poles and dissociates as growth is terminated. It then reappears at the new pole sites (top). During FtsA depletion, FtsZ-sfGFP forms rings marking the future sites of pole formation (bottom). All scale bars are set to 2 μm.

Movie 2. Growth and morphological changes during FtsA depletion. Cells were washed to remove inducer and grown in liquid ATGN for 2 hours before spotting on a ATGN pad. Images were acquired every ten minutes and movie is played at 10 frames per second for a total of 97 frames.

Figure 9. FtsW is not required for termination of polar growth A) Timelapse microscopy shows cells expressing FtsW grow and divide normally forming microcolonies (top panel). Cells depleted of FtsW terminate polar growth and form new growth poles near the mid-cell (bottom panel). B) FDAA labels a single growth pole when FtsW is present (top) and labels multiple poles emerging from the mid-cell when FtsW is absent (bottom). C) Timelapse microscopy during FtsW depletion shows PopZ-YFP localizes to the growth poles and dissociates as growth is terminated. It then reappears at the new pole sites (top). During FtsW depletion, FtsZ-sfGFP forms rings marking the future sites of pole formation (bottom).

Movie 3. Growth and morphological changes during FtsW depletion. Cells were washed to remove inducer and grown in liquid ATGN for 4 hours before spotting on a ATGN pad. Images were acquired every ten minutes and movie is played at 10 frames per second for a total of 85 frames.

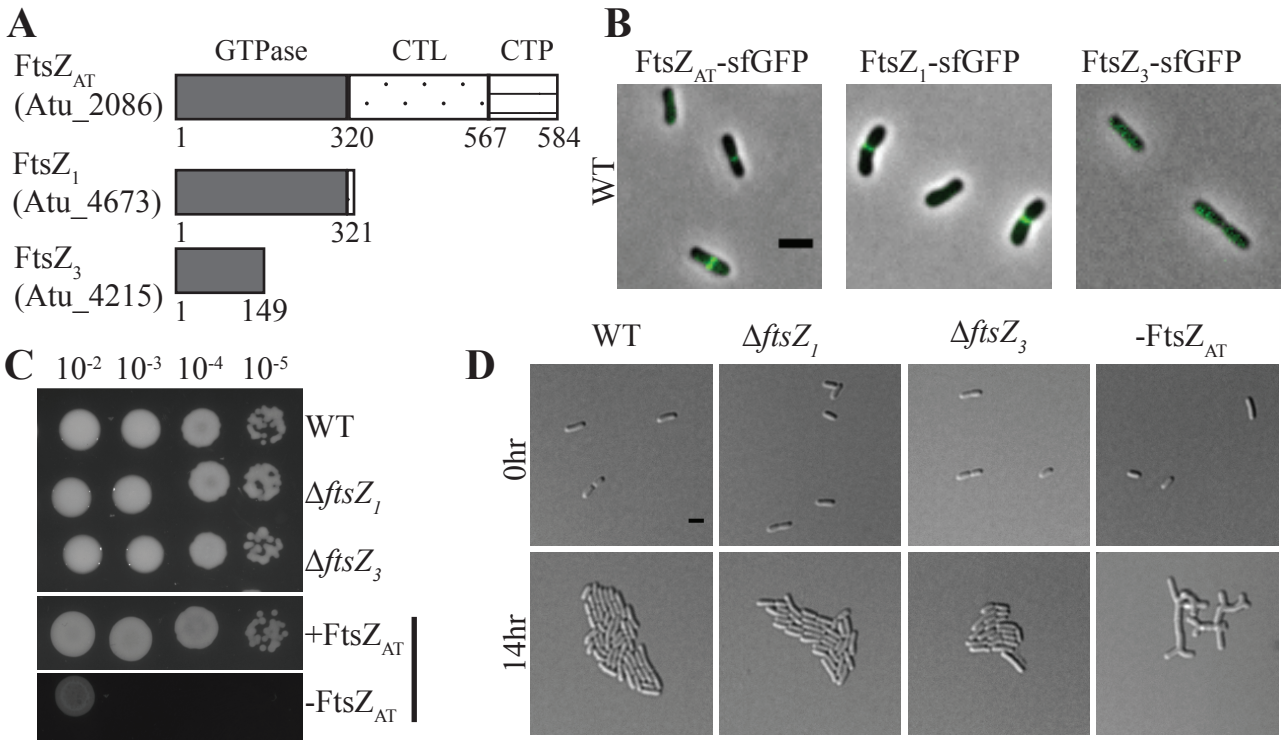

Figure 1

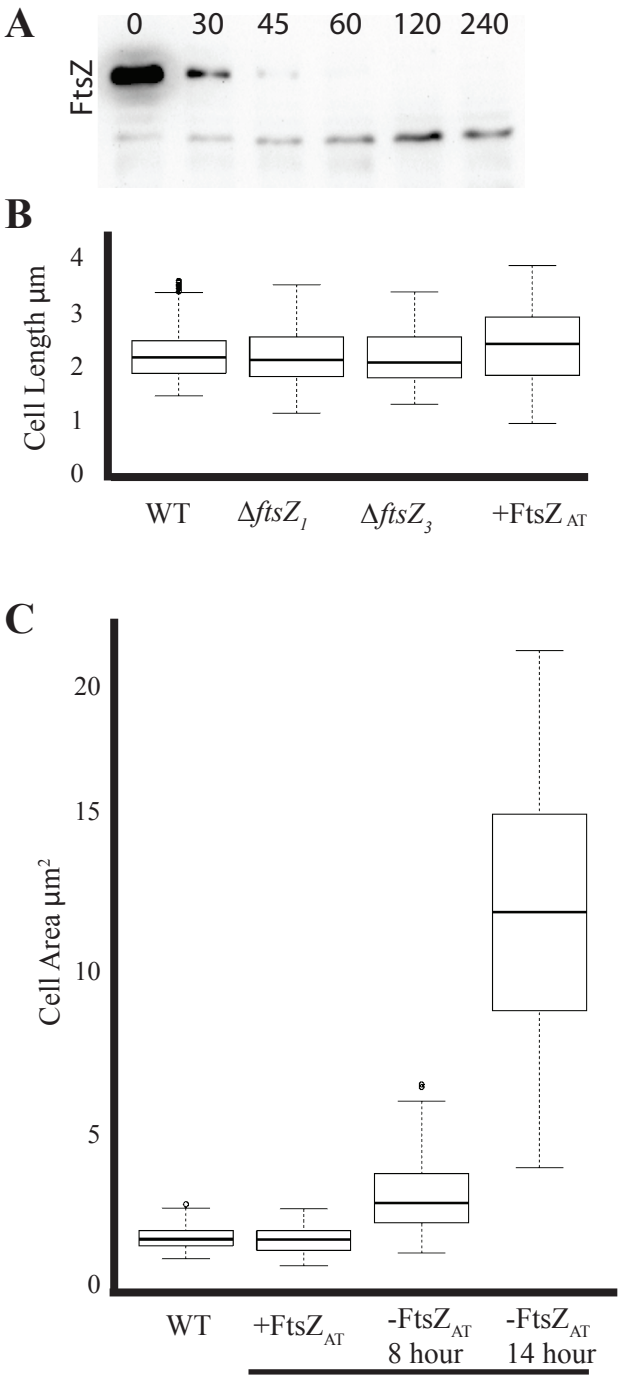

Figure 1- Figure Supplement 1

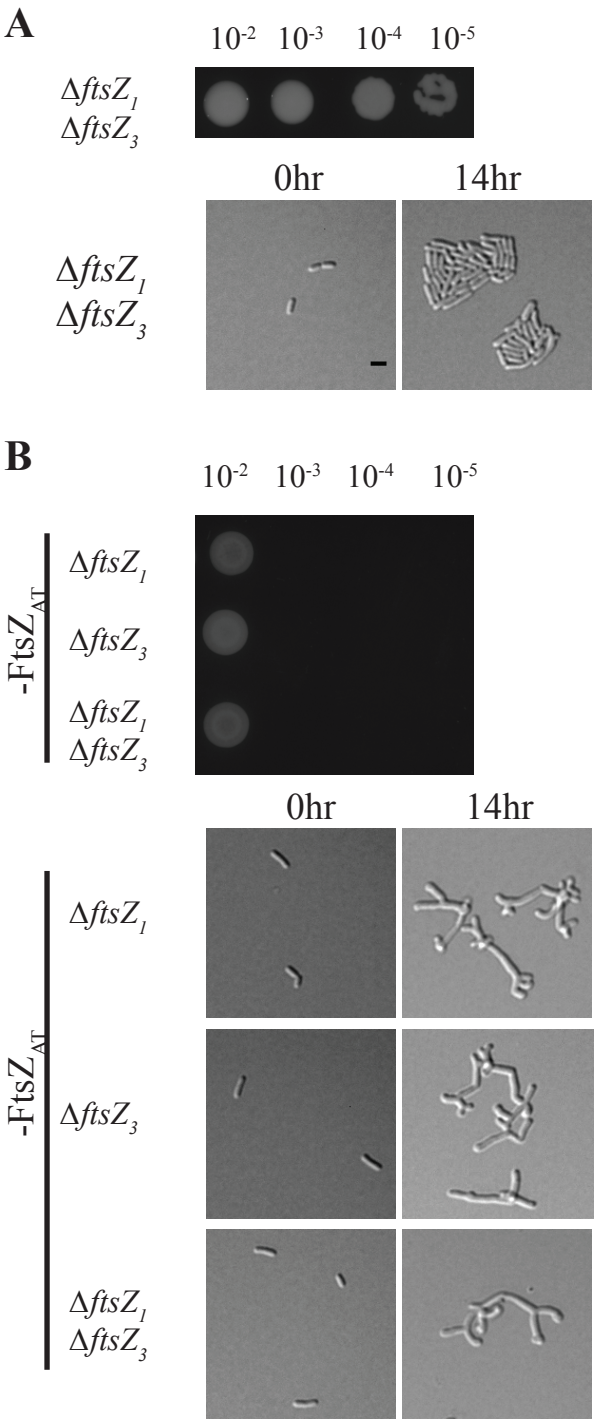

Figure 2

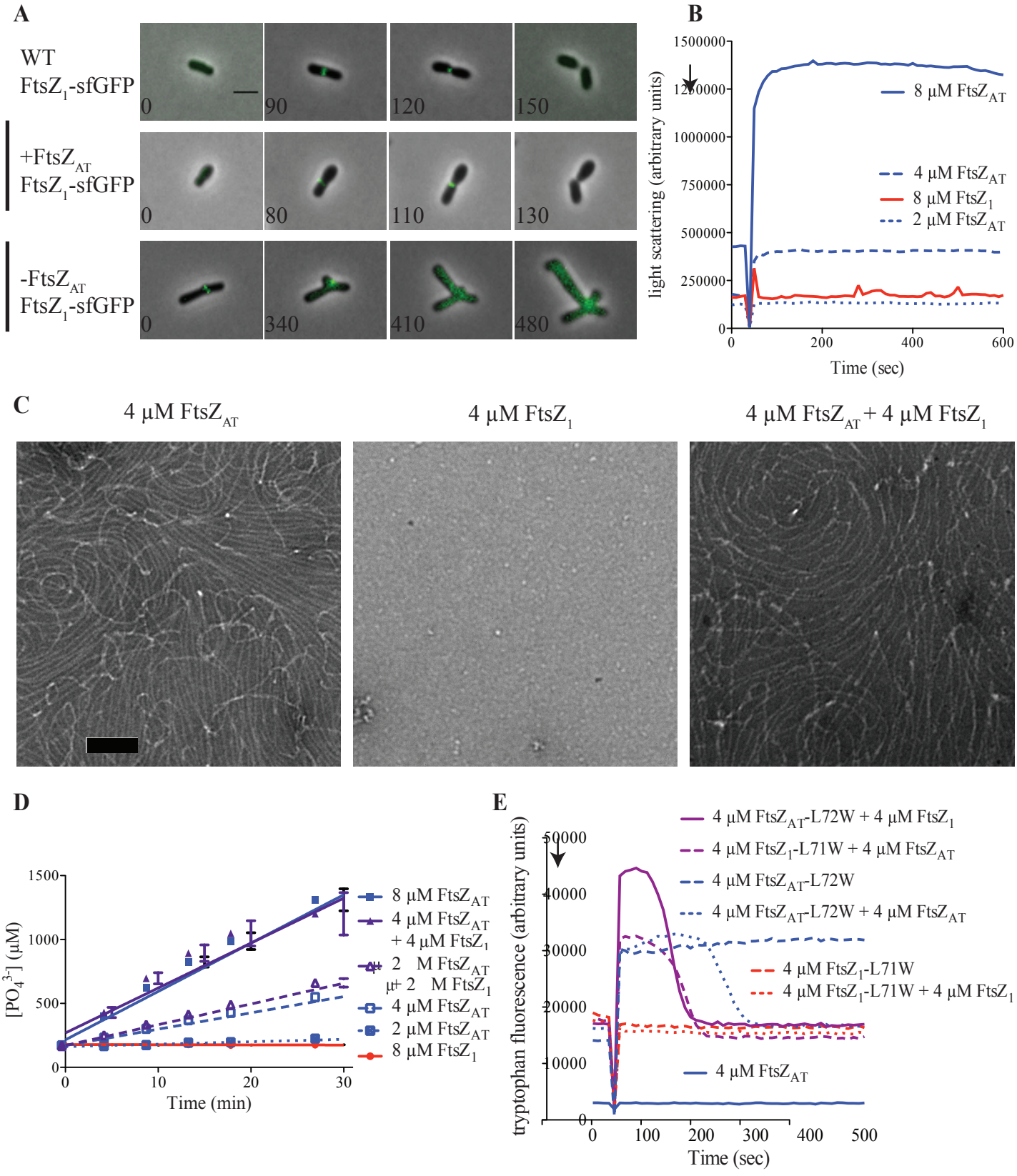

Figure 3

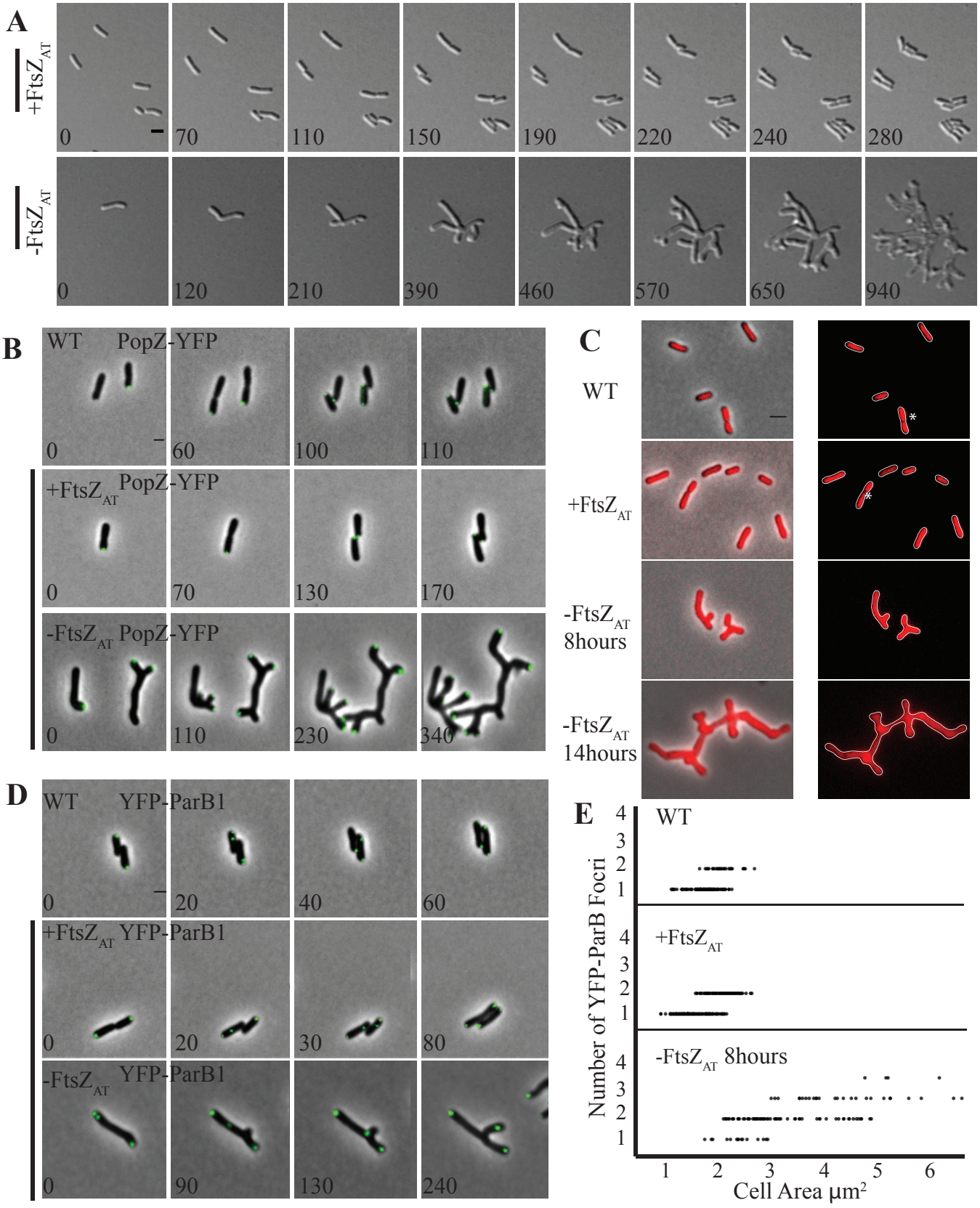

Figure 4

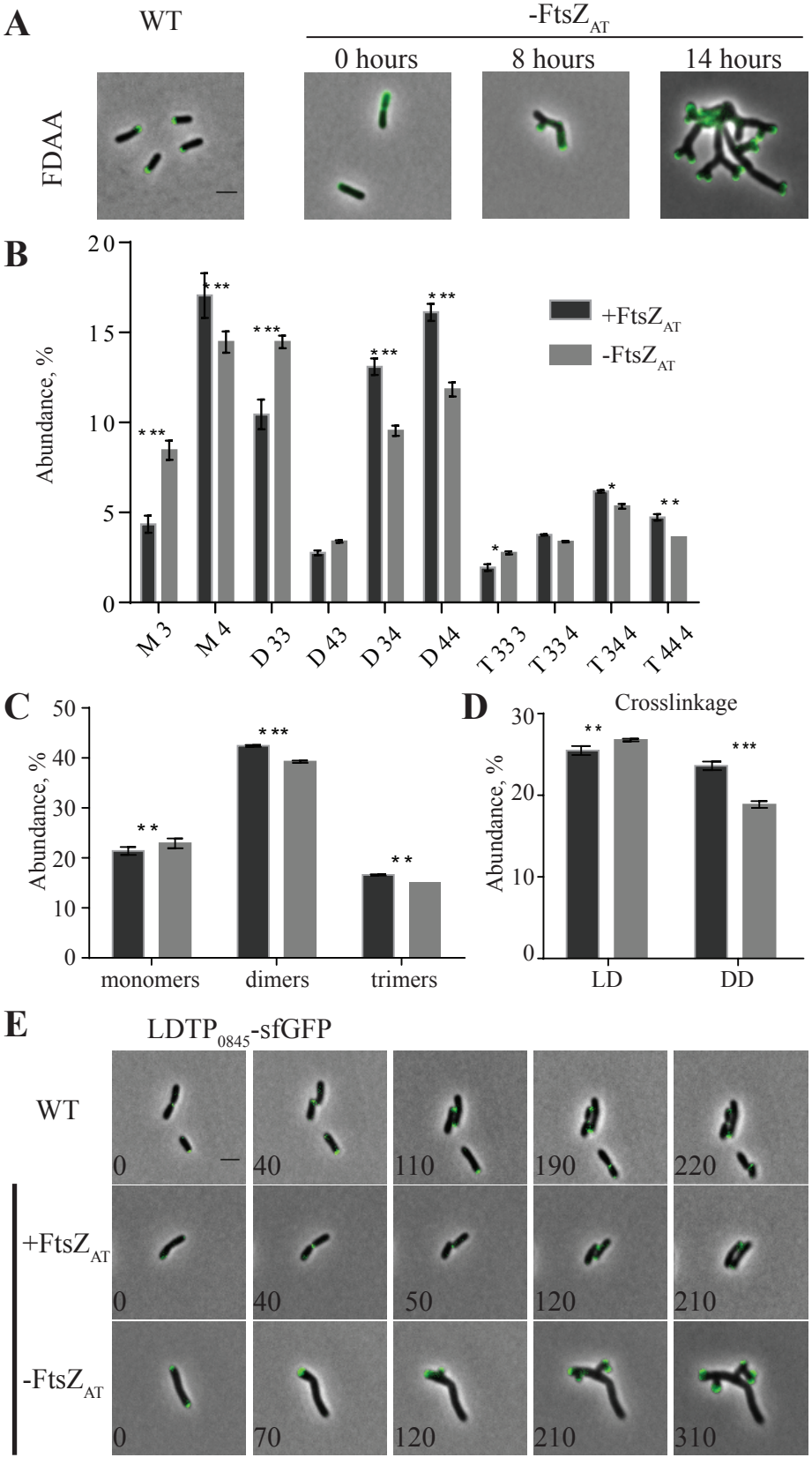

Figure 5

A

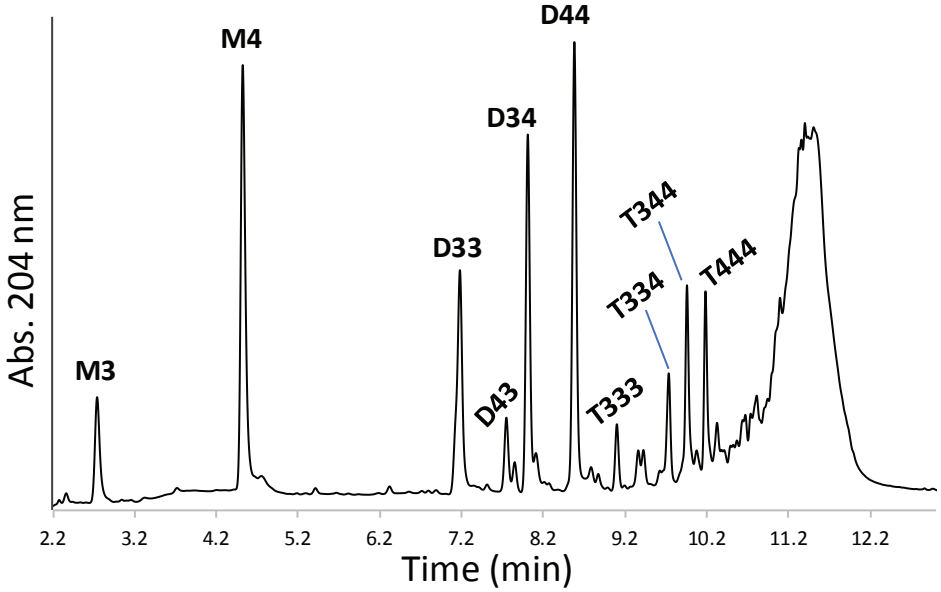

B

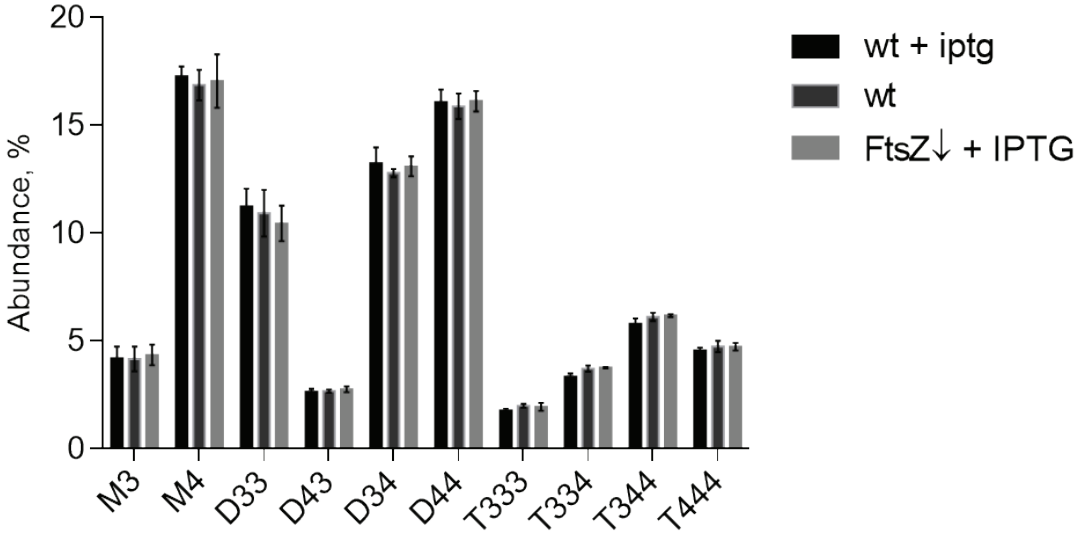

Figure 5- Figure Supplement 1

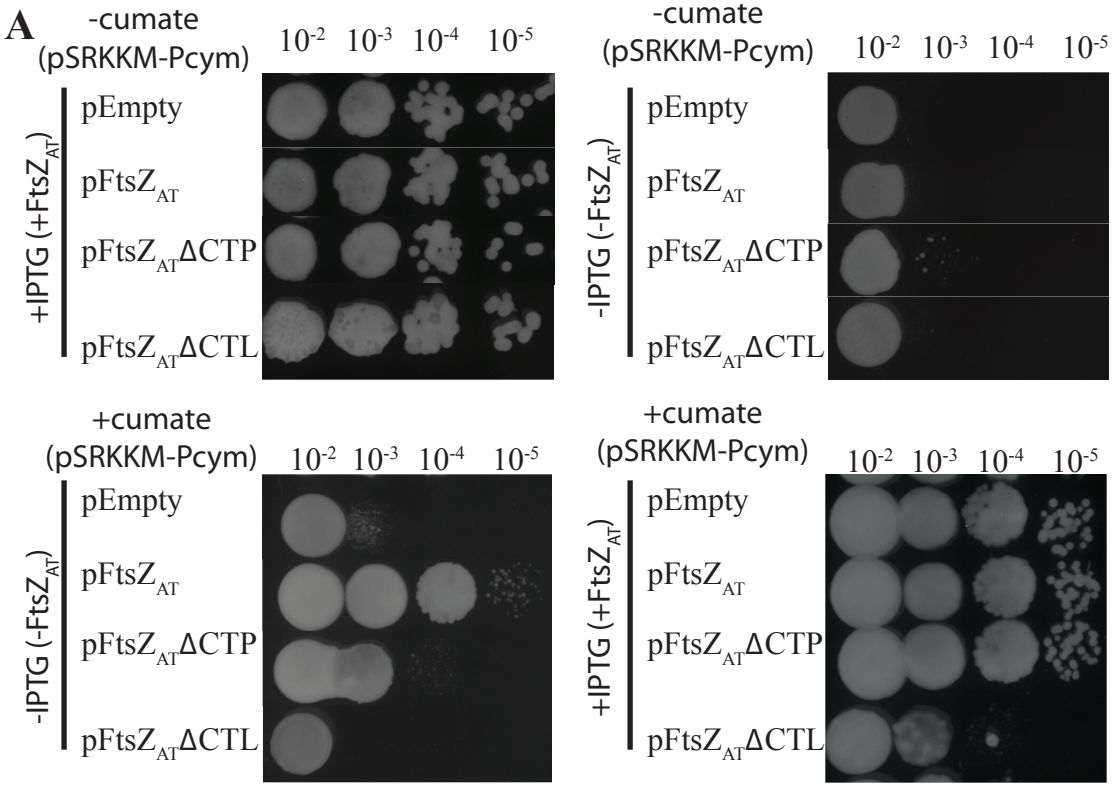

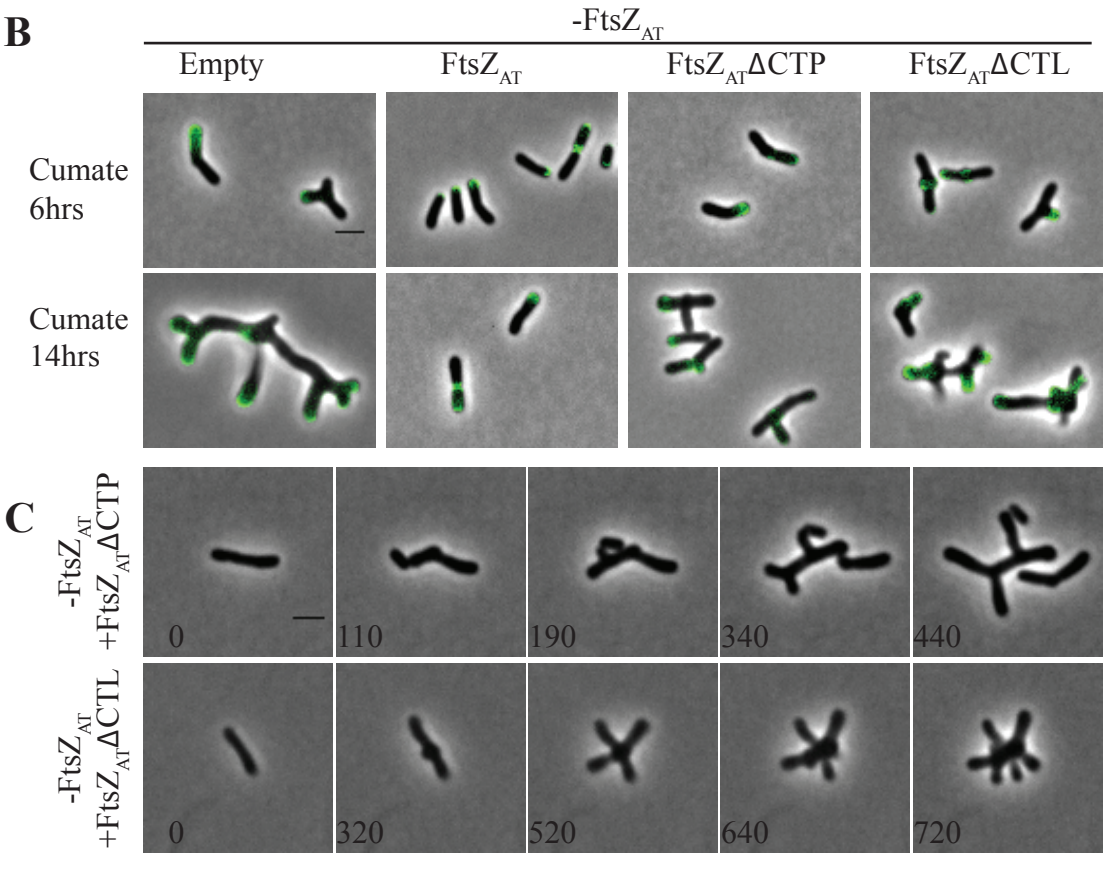

Figure 6

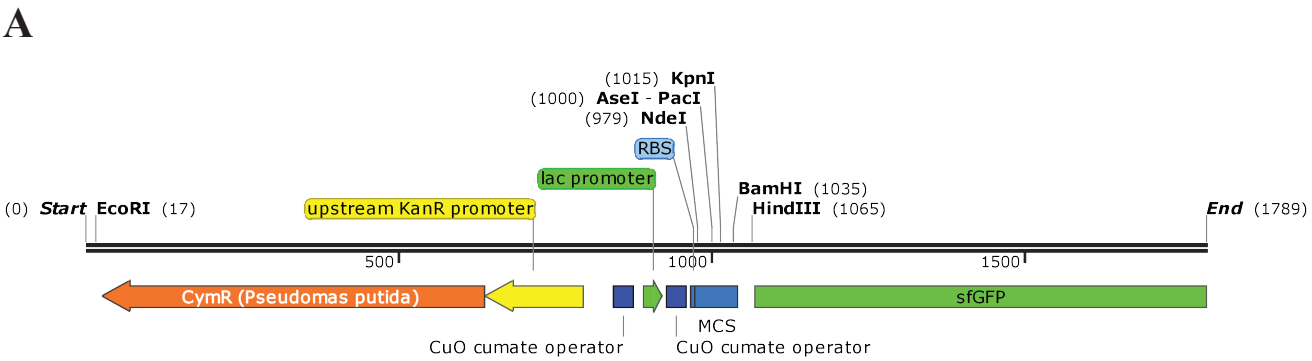

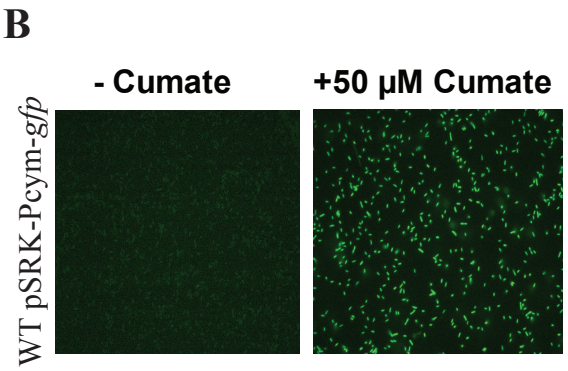

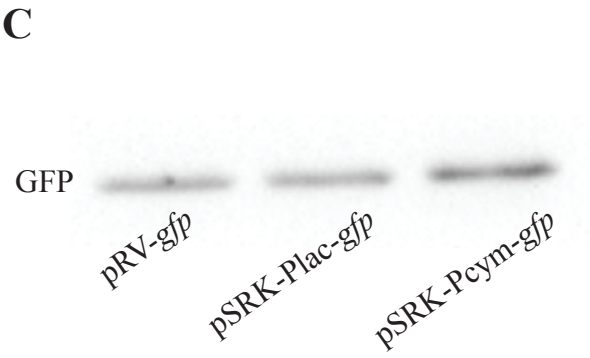

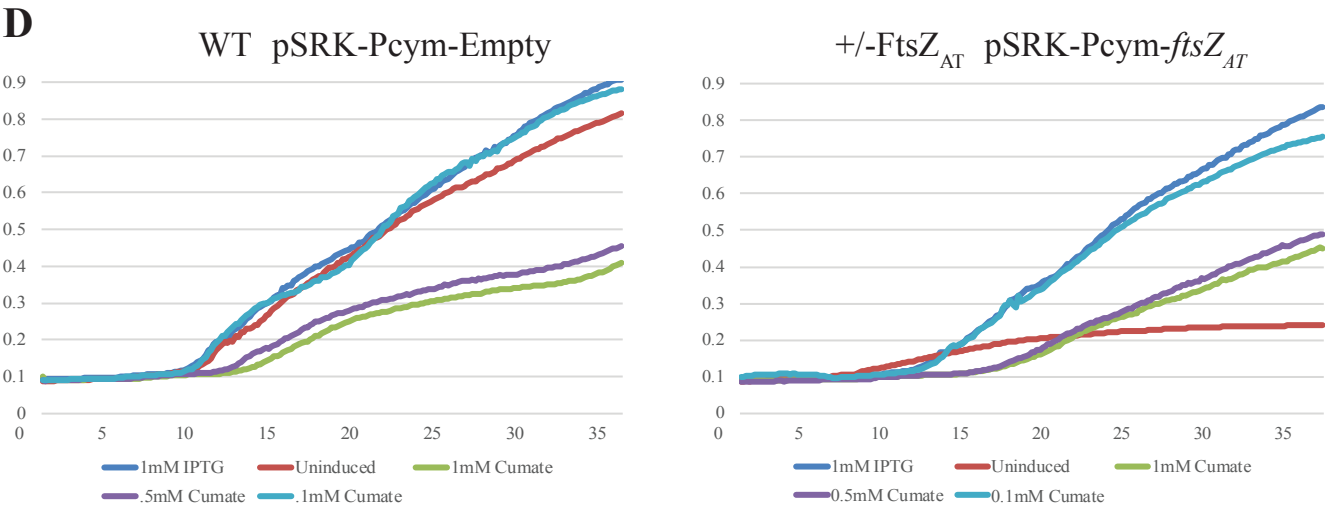

Figure 6- Figure Supplement 1

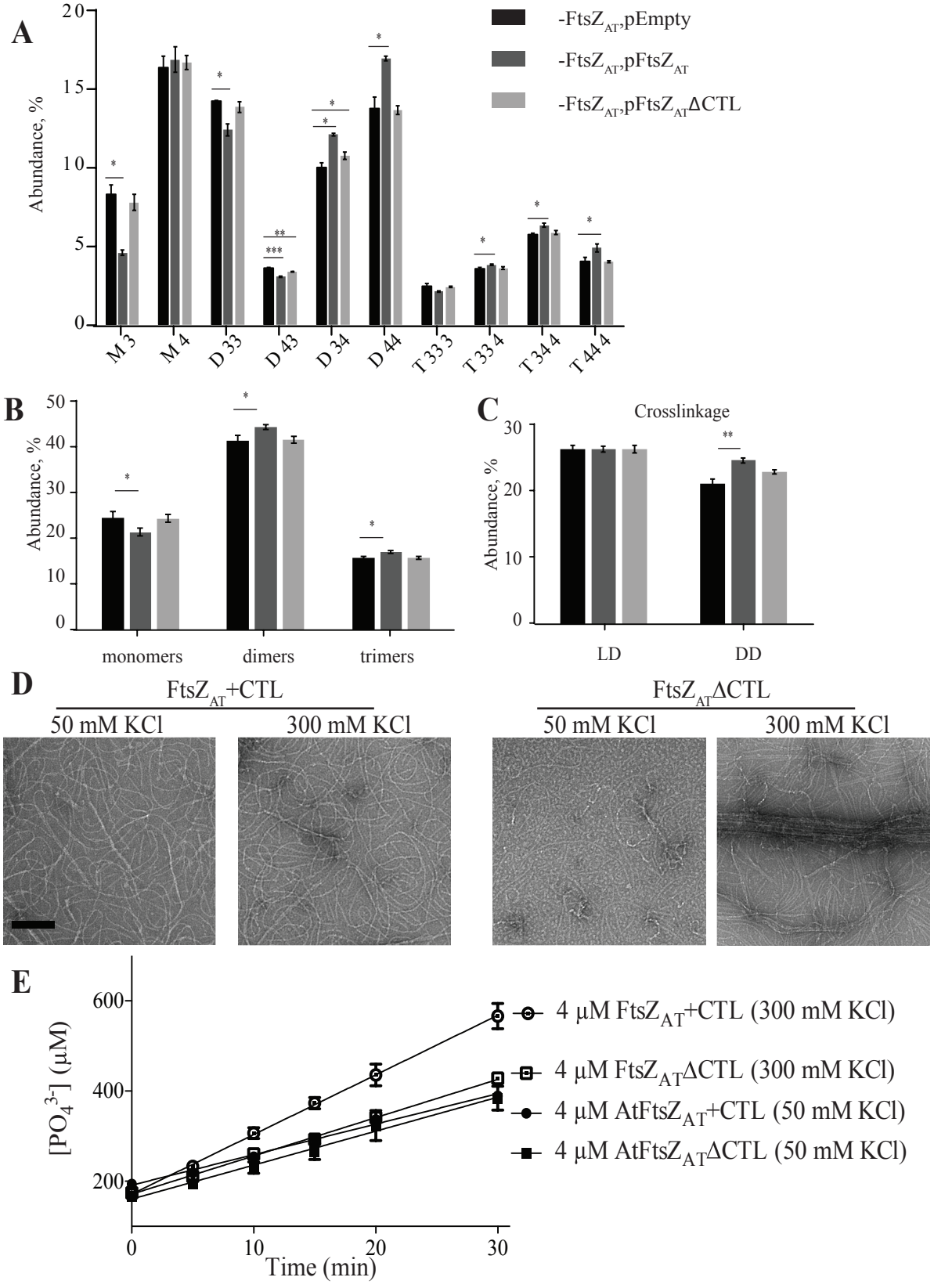

Figure 7

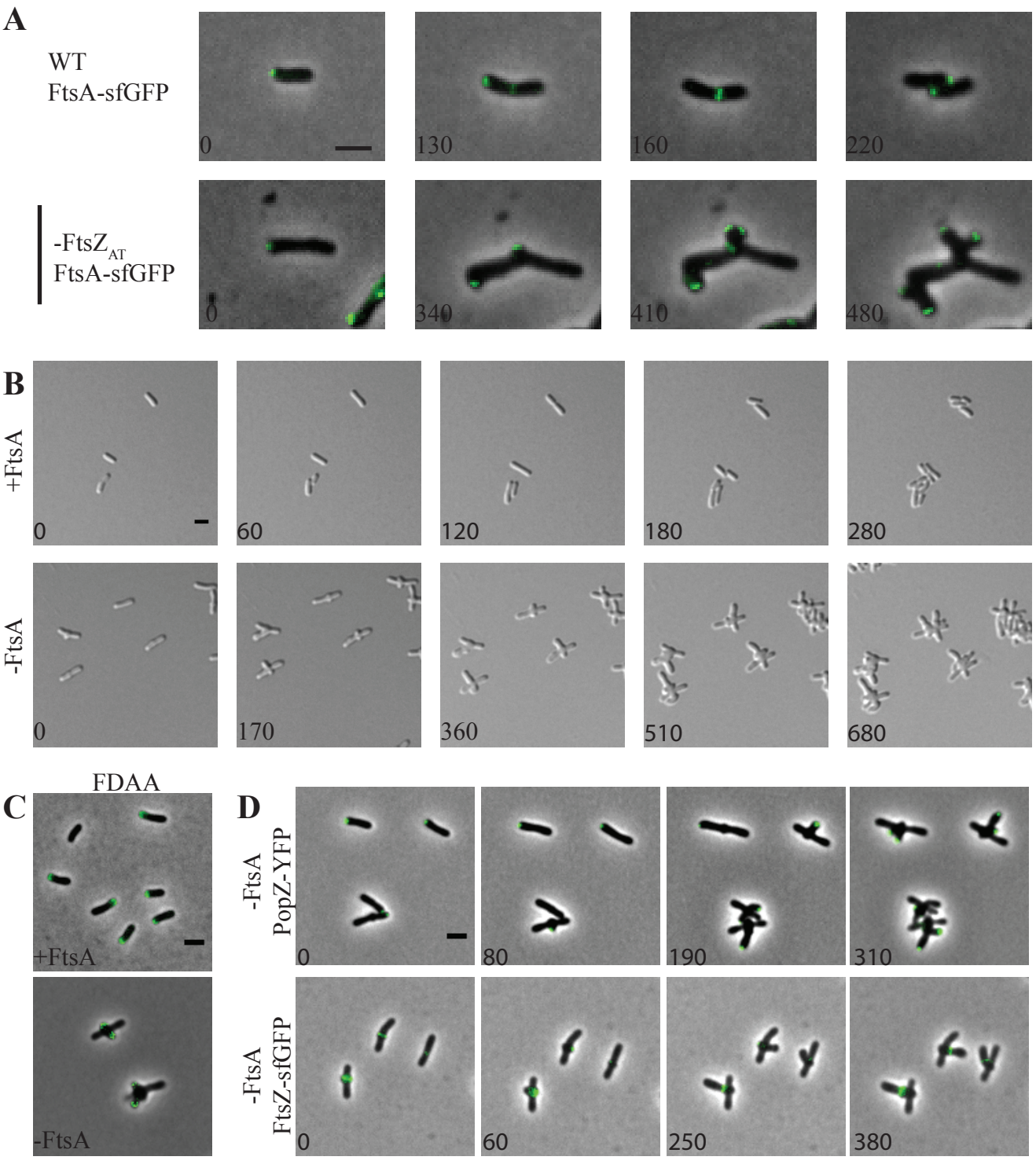

Figure 8

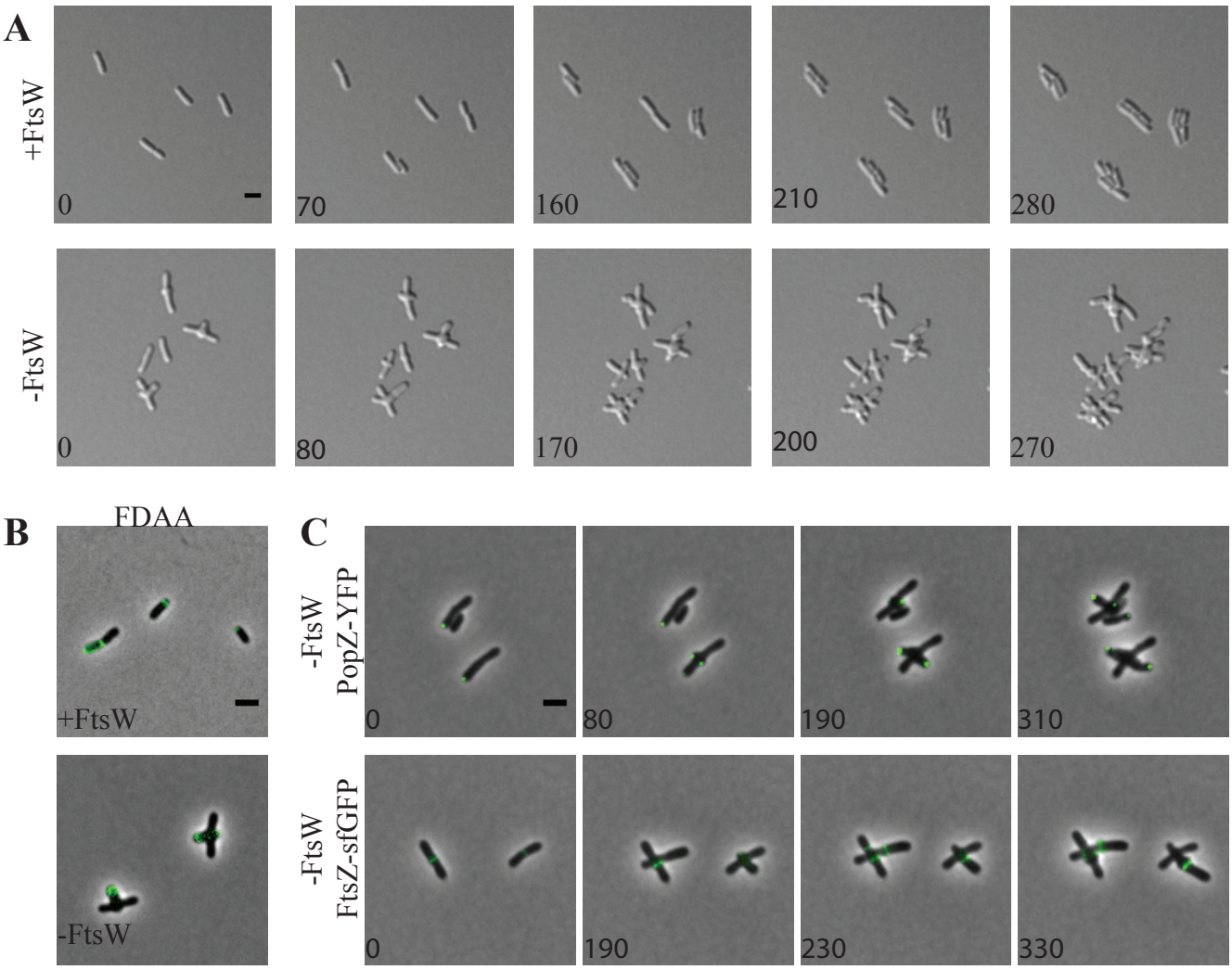

Figure 9